Joule

Article

Geological ammonia: Stimulated NH_3 production from rocks

Graphical abstract

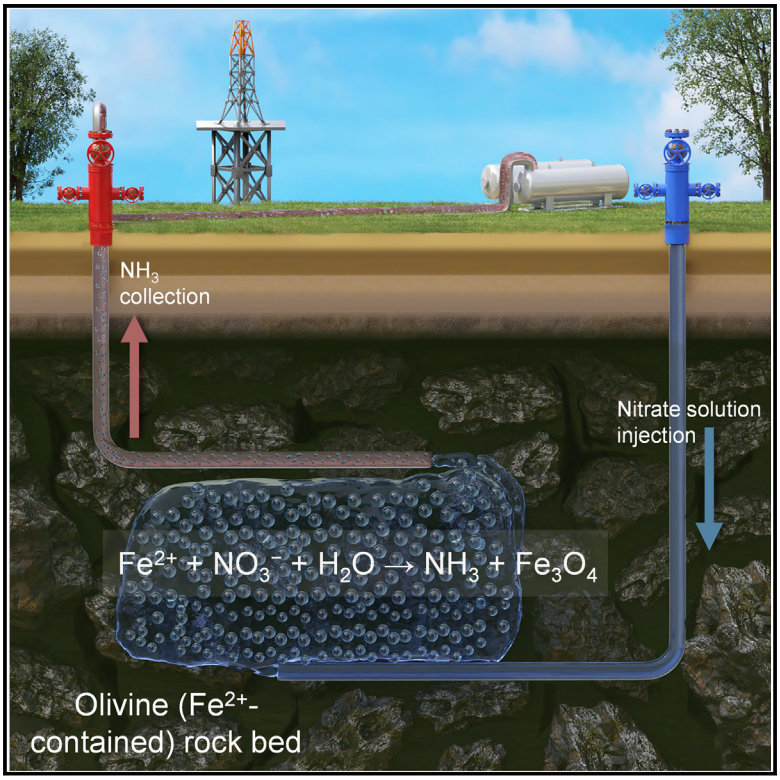

Highlights

- Stimulated and *in situ* geological NH_3 as a new approach for NH_3 production at scale
- NH_3 is produced by injecting nitrate-containing water into iron-rich formations
- Using Cu^{2+} as a catalyst, 1.8 kg NH_3/t olivine was produced at 300°C in 21 h
- This approach requires no external H_2 or electric current and emits no direct CO_2

Authors

Yifan Gao, Ming Lei, Bachu Sravan Kumar, ..., Lokesh Sangabattula, Ju Li, Iwnetim I. Abate

Correspondence

yifangao@mit.edu (Y.G.), liju@mit.edu (J.L.), iabate@mit.edu (I.I.A.)

In brief

Ammonia (NH_3) is the most produced chemical globally and a major contributor to greenhouse gas emissions. Here, we propose and demonstrate a different approach, where NH_3 is produced by injecting nitrate-containing water into iron-rich formations. This process does not require H_2, electricity, or application of external temperature or pressure and emits no direct CO_2. Our work paves the way for using Earth's subsurface as a reactor, with abundant rocks as feedstock, to theoretically produce enough NH_3 for 2.42 million years.

Gao et al., 2025, Joule 9, 101805
February 19, 2025
https://doi.org/10.1016/j.joule.2024.12.006

CellPress

Joule

CellPress

Article

Geological ammonia: Stimulated NH_3 production from rocks

Yifan Gao,[1,*] Ming Lei,[1] Bachu Sravan Kumar,[1] Hugh Barrett Smith,[1] Seok Hee Han,[1] Lokesh Sangabattula,[1] Ju Li,[1,2,*] and Iwnetim I. Abate[1,3,*]

[1]Department of Materials Science and Engineering, Massachusetts Institute of Technology, Cambridge, MA 02139, USA
[2]Department of Nuclear Science and Engineering, Massachusetts Institute of Technology, Cambridge, MA 02139, USA
[3]Lead contact
*Correspondence: yifangao@mit.edu (Y.G.), liju@mit.edu (J.L.), iabate@mit.edu (I.I.A.)
https://doi.org/10.1016/j.joule.2024.12.006

CONTEXT & SCALE Ammonia (NH_3) is the most produced chemical globally and a major contributor to greenhouse gas emissions, largely due to the energy-intensive Haber-Bosch process. Alternative methods are needed to achieve cost parity, CO_2 reduction, independence from critical minerals, and decentralized NH_3 production. Here, we propose and demonstrate a completely different approach, where NH_3 is produced by injecting nitrate-containing water into iron-rich formations. Through a chemical redox reaction, ferrous iron in the rock converts nitrate into NH_3 under ambient conditions and subsurface heat and pressure (130°C–300°C and 0.25–8.5 MPa). This geological process does not require H_2, electricity, or application of external temperature or pressure, and emits no CO_2. Our work paves the way for using Earth's subsurface as a reactor, with abundant rocks as feedstock, to theoretically produce enough NH_3 for 2.42 million years while minimizing environmental impact and achieving sustainability and decarbonization in the chemical and energy sectors.

SUMMARY

Although ammonia production is crucial for global agriculture, it comes with substantial carbon footprints. Here, for the first time, we propose and demonstrate a different method for stimulated (proactive) and *in situ* geological ammonia (Geo-NH_3) production directly from rocks. Our approach demonstrated that NH_3 can be efficiently generated by reacting natural $(Fe,Mg)_2SiO_4$ (olivine) minerals with nitrate-source water at 130°C–300°C and 0.25–8.5 MPa, and even at ambient temperature and pressure. Using both actual rocks and synthetic mineral $Fe(OH)_2$, we investigated mechanisms and optimized conditions through experiments and theoretical calculations. We revealed the basic chemistry enabling Geo-NH_3 production: Fe^{2+} contained in rocks reduces the nitrate source to NH_3. Our approach, involving only the injection of nitrate-source water into the subsurface to utilize *in situ* subsurface heat and pressure, requires no external H_2 or electric current and emits no direct CO_2, offering a feasible alternative to sustainable NH_3 production at scale.

INTRODUCTION

Ammonia (NH_3) is one of the most produced chemicals, and the industrial process of synthesizing it accounts for approximately 2% of global energy consumption and 1.3% of CO_2 emissions.[1] The majority of produced NH_3 is used for fertilizers (about 70%), with the remainder utilized in producing plastics, explosives, synthetic fibers, etc.[2] Moreover, NH_3 will play a critical role in the green energy transition, as a clean energy carrier/fuel,[3] to decarbonize energy-intensive industries[4] and transportation (as a clean fuel for ships[5] and airplanes[6]). It is also considered an alternative to hydrogen fuel due to its relative ease of liquefaction and transportation.[7] The discovery and established infrastructure of the Haber-Bosch process addressed the technical problems of large-scale production of fertilizers.[8] However, this method emits around 450 million tonnes (Mt) of CO_2 per year and 2.4 tonnes CO_2 per tonne NH_3 produced, making it the highest CO_2 emitter in the chemical industry.[9] Steel and cement production account for only a half and a quarter of emissions, respectively, compared with NH_3 production.[10] A significant portion of the CO_2 emitted during the Haber-Bosch process (approximately 70%–80%) is due to the black/gray H_2[11] used in the reaction, which is produced from the steam reforming of coal or natural gas ($CH_4 + 2H_2O \rightarrow 4H_2 + CO_2$). The rest of the CO_2 partially comes from the natural gas used to create and sustain the high temperature and pressure required for the reaction,

350°C–450°C and 150–200 atm, respectively. Another key challenge posed by the Haber-Bosch process is the centralized nature of production due to the intense capital and energy needed.

Recently, significant strides have been made in electrochemical NH_3 (green NH_3) production, promising to decentralize production and reduce CO_2 emissions.[12–14] However, this method requires electricity to run the electrolyzers, ideally sourced from renewables such as wind and solar. Yet, the intermittent nature of renewable energy necessitates battery storage to ensure the continuous operation of electrolyzers. As a result, electricity production adds to NH_3 production costs, potentially making it less competitive than the Haber-Bosch process.[15] Furthermore, to produce NH_3 at scale (expected to rise from 180 Mt/year in 2020 by 30% by 2050[16]), a substantial amount of mining, including critical minerals, is necessary for the production of wind turbines, solar cells, batteries, and electrolyzers, which is prone to significant CO_2 emission and supply chain challenges. Projections on electrochemical production of H_2 (which shares similar challenges in scaling up as electrochemical production of NH_3) suggest that meeting all H_2 demands through this method would necessitate the utilization of all solar and wind energy projected to be on the grid in 2050. This would require intensive mining of critical minerals such as lanthanum, yttrium, or iridium for electrolyzers and neodymium, silicon, zinc, molybdenum, aluminum, lithium, nickel, and copper to construct dedicated renewable electricity sources.[17] Although H_2 is not required for the production of NH_3 from electrocatalytic reduction of nitrate, challenges remain due to the need for high conductivity and high nitrate concentrations in the feedstock solution, as well as the consumption of electrical energy.[13] In addition, although using nitrate from wastewater and agricultural runoff for NH_3 production cannot fully replace the Haber-Bosch process, this sustainable route for NH_3 production has been recognized in many studies, particularly in utilizing electrocatalytic nitrate reduction with transition metal catalysts.[13,14,18–21] As a result, alternative methods need to be explored to replace the incumbent production pathway for NH_3, achieving cost parity, CO_2 reduction goals, independence from critical minerals, and decentralization of NH_3 production at scale during the green energy transition.

"Natural H_2" or "geological H_2" is emerging as an alternative pathway to alleviate the challenges associated with the electrochemical production of H_2. It is produced by a chemical redox reaction known as serpentinization, where Fe-containing rocks (ultramafic rocks) oxidize while reducing underground water to H_2.[22] The subsurface provides the necessary heat and pressure for this thermochemical reaction (approximately 50°C–350°C and up to 20–35 MPa[23]). Even though there are large untapped reservoirs of natural H_2, ranging from ~0.5 to >1,000 Mtpa of H_2 (referred as "white H_2"),[17,23] recently, methods to stimulate the reaction for *in situ* generation and harvesting of natural H_2 are being explored (referred as "orange H_2"[11]). This pathway is anticipated to cost less than $1/kg[24] (cheaper than black/gray H_2 at approximately $2/kg), with no apparent direct CO_2 emissions, while avoiding mineral supply constraints associated with green H_2. Inspired by orange H_2, in this work, we demonstrate a novel method to produce stimulated orange-NH_3, i.e., geological NH_3 (Geo-NH_3). If scaled, this process would have near-zero CO_2 emissions and face no mineral supply chain constraints. Although there are earlier reports focused on the passive observation of NH_3 generation from rocks[25–32] (primarily in the context of the origin of life and the natural nitrogen cycle), this work is the first to demonstrate stimulated (proactive) and *in situ* Geo-NH_3 production as a potential alternative technology for NH_3 synthesis. By systematically studying this reaction under controlled parameters such as temperature, pressure, and catalysts, we offer the first structured approach to understanding and optimizing stimulated Geo-NH_3 production.

In this work, to produce Geo-NH_3, we modified the serpentinization reaction by exposing the rock not only to water but also to nitrate (NO_3^-) in the presence of a catalyst (Cu^{2+} or Ni^{2+}). By systematic controlled experiments and isotope testing, we confirmed the generation of NH_3 from both olivine (1,752.6 ± 96.9 g NH_3/t olivine) and synthetic mineral ($Fe(OH)_2$) (10.4 ± 0.5 kg NH_3/t $Fe(OH)_2$), which is the $Fe(OH)_2$ involved in the last step in the serpentinization reaction. If scaled, this technology could achieve an equivalent field production rate of approximately 40,000 tonnes of NH_3 per well from rocks containing olivine. Gas chromatography analysis revealed that although the catalyst enhances the rate of H_2 production by over 50 times, in the presence of nitrate, no H_2 is produced, confirming direct conversion to NH_3. We achieved these reactions at both ambient conditions and temperatures of 90°C–300°C and pressures of 0.25–8.5 MPa, with the possibility of increasing the yield and rate with higher temperature and pressure upon further reaction optimization. X-ray diffraction and X-ray photoemission spectroscopy confirmed the transformation from Fe^{2+} to Fe^{3+} in Fe_3O_4 during the chemical redox process that generates NH_3. We have also performed first-principles calculations to elucidate the reaction mechanism and conducted a techno-economic analysis to compare the proposed technology with other competitive alternatives. Our Geo-NH_3 approach, which involves injecting nitrate-containing water into the subsurface to leverage *in situ* heat and pressure, requires no external hydrogen or electricity and emits no CO_2. This method presents a viable, scalable alternative for sustainable NH_3 production at a competitive cost.

RESULTS AND DISCUSSION

Subsurface reaction system to generate "natural ammonia" or "geological ammonia"

The pathway of H_2 production from rocks, called serpentinization process,[22,33] is currently explained mainly by the following reaction processes (Equations 1–4):

$$(Fe,Mg)_2SiO_4\ (\text{olivine}) + H_2O \rightarrow (Fe,Mg)_6Si_4O_{10}(OH)_8\ (\text{serpentine}) + (Mg_{1-x},Fe_x)(OH)_2\ (\text{Fe-bearing brucite}) + Fe_3O_4\ (\text{magnetite}) + H_2 \quad \text{(Equation 1)}$$

$$(Mg_{1-x},Fe_x)(OH)_2 + H_2O \rightarrow (1-x)\ Mg^{2+} + x\ Fe^{2+} + 2OH^- \quad \text{(Equation 2)}$$

$$Fe^{2+} + 2OH^- \rightarrow Fe(OH)_2 \quad \text{(Equation 3)}$$

$$3Fe(OH)_2 + 2\ H_2O \rightarrow Fe_3O_4 + H_2 + 4H_2O \quad \text{(Equation 4)}$$

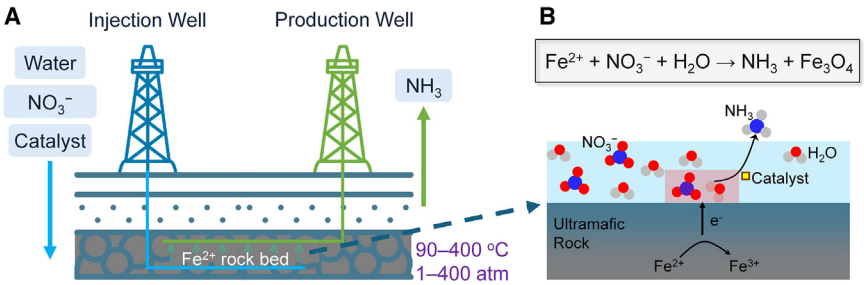

Figure 1. Schematic and configuration of the abate cycle, the subsurface thermochemical redox reaction for ammonia synthesis

(A) It comprises several components, including an injection well, fluid delivery apparatus, flow passages (boreholes), and a production well. These components are interconnected for fluid communication. Additional elements, like pumps, may be employed to regulate compound flow. Water, nitrate (NO_3^-), and additives (e.g., catalyst, pH agent, etc.) flow toward the ultramafic rock bed through the first borehole (blue arrows). After redox reactions on the rock surface, NH_3 exits the subsurface through the second borehole (green arrow) to be collected at the surface (can be collected either in a gas form or as NH_3 dissolved in water).

(B) Schematic of reaction at the rock-fluid interface where the Fe^{2+} in the rock is oxidized while reducing NO_3^- into NH_3.

In principle, the production of H_2 relies on the redox reaction between the ferrous iron (Fe^{2+}) and water. Inspired by this, we aim to utilize the reduction potential of ferrous iron in rocks, but, instead of reducing water, we seek to reduce nitrate (NO_3^-) with the expectation of producing NH_3. The following reaction equation (Equation 5) describes the proposed chemical basis of Geo-NH_3 production: nitrate in aqueous solution is reduced by Fe^{2+} present in (or transformed from) the rock to generate NH_3, while Fe^{2+} is oxidized to Fe_3O_4.

$$Fe^{2+} + NO_3^- + H_2O \rightarrow NH_3 + Fe_3O_4 \quad \text{(Equation 5)}$$

As shown in Figure 1, we propose a surface thermochemical redox reaction process for NH_3 synthesis, "the abate cycle," aiming at controlling the reaction and discovering and using catalysts to enhance the Geo-NH_3 production rate. This process involves injecting a nitrate aqueous solution into the ground to react with ferrous-containing rocks, producing a solution containing NH_3 that will be collected back above ground (Figure 1A). This system is designed with multiple components essential for the operation, including a fluid delivery apparatus, a reservoir tank, flow passages known as boreholes, and a collection tank. To manage the flow of compounds effectively, additional equipment such as pumps may be incorporated. The process initiates with the conveyance of water, nitrate (NO_3^-), and various additives—such as catalysts and pH-adjusting agents—toward an ultramafic rock bed via the first borehole, as indicated by blue arrows. These additives are crucial for facilitating the redox reaction on the rock's surface. Following this reaction, Geo-NH_3 is produced and then exits the subsurface through a second borehole, illustrated by a green arrow, where it is subsequently collected at the surface. The water and its additives can be recycled to reduce costs and environmental impact. In future mini and pilot field tests, similar processes to those used in shale gas will be drawn upon to avoid plugging and increase rock permeability, for example, by increasing the pressure of hydraulic fracturing. Conditions will also need to be optimized to reduce the occurrence of side reactions to increase yield.

A closer examination of the reaction mechanics, as depicted in Figure 1B, reveals the interaction at the rock-fluid interface. Here, ferrous iron (Fe^{2+}) present in the rock undergoes oxidation. Simultaneously, this oxidative process results in the reduction of nitrate (NO_3^-) into NH_3. The principle is similar to that of all NH_3 synthesis methods,[13,14,18–21] which are based on oxidation-reduction chemistry. But it is worth highlighting that this work proposes, for the first time, the processes of stimulated (proactive) and *in situ* Geo-NH_3 production, which are different from previous NH_3 production processes (see Note S1 for more discussion).

Measurement of geological ammonia generation

A laboratory-scale rock-water reaction system was set up to produce Geo-NH_3 (Figure S1), which is very similar to the application scenario illustrated in Figure 1. During low-temperature serpentinization reactions (90°C to 200°C), ultramafic rocks, such as those with high olivine ($(Fe,Mg)_2SiO_4$) contents, undergo a series of chemical transformations when exposed to H_2O.[34,35] First, the reaction leads to the release of dissolved ions such as Mg^{2+} and Fe^{2+}. Second, Fe^{2+} undergoes a transformation to form $Fe(OH)_2$. Finally, a significant aspect of this process involves the generation of H_2 gas during the oxidation of Fe^{2+} within $Fe(OH)_2$ to form Fe_3O_4 (magnetite).[36–38] Therefore, in addition to the actual olivine samples, we investigated the feasibility and reaction mechanisms—and optimized the conditions—of using $Fe(OH)_2$ as a simulated mineral of rock. The goal was to assess both NH_3 and H_2 gas production capabilities under controlled conditions. The initial reaction of $Fe(OH)_2$ with water at 90°C and atmospheric pressure yielded trace amounts of H_2 gas, detectable through gas chromatography (GC) analysis, as illustrated in Figure 2A along with its magnified inset.

To enhance the rate and yield of H_2 production, we introduced Ni^{2+} as a catalyst into the $Fe(OH)_2$ matrix equivalent to 1% of the $Fe(OH)_2$ mass. Surprisingly, the inclusion of this small quantity of Ni^{2+} significantly accelerated H_2 gas production, as depicted in Figure 2A. This result first confirmed our hypothesis that geological H_2 could be generated from rock-water reactions. The peak of the reaction occurs after around 1 h and approaches equilibrium at 5–6 h.

Upon adding sodium nitrate to the reaction mixture, still containing Ni^{2+}, the H_2 production markedly decreased to nearly zero, even falling below the levels observed in the absence of Ni^{2+}. Subsequent analysis of the reaction products indicated the oxidation of Fe^{2+} to Fe^{3+} (see the next section for more discussion). When H_2 gas was not produced, the electrons from

the oxidation of Fe^{2+} needed an alternative acceptor. The most likely candidate was the added nitrate, which was presumed to be reduced. This hypothesis was confirmed through nuclear magnetic resonance (NMR) analysis of the post-reaction solution (Figure 2B), which identified the distinct spectral lines of NH_4^+. This equates to the production of 7.7 ± 0.4 kg NH_3 per tonne of $Fe(OH)_2$. Thus, we demonstrated that Geo-NH_3 could be produced from representative rock-like chemical substances.

Further experiments were conducted using actual mineral samples, specifically olivine. Initial tests at 130°C and 0.25 MPa, without adding nitrate, also observed H_2 production (Figure 2C), verifying successful Geo-H_2 generation. It is worth noting that in this work we produced H_2 from actual minerals at a rate of 0.32 μmol g^{-1} h^{-1}, which is nearly 10 times higher than previous reports.[39] The successful and efficient production of Geo-H_2 from actual mineral samples corroborates the scientific validity of our methodology and also underscores the application potential. This flexibility, demonstrated by the ability to adjust production toward either Geo-H_2 or Geo-NH_3 as necessitated by application demands, heralds a significant stride in the endeavor to harness geological processes for sustainable energy production. The introduction of nitrate into this system resulted in very low hydrogen production (Figure 2C and Note S2) and the detection of NH_4^+ (Figure 2D), demonstrating that each tonne of olivine could produce 38.5 ± 3.1 g of NH_3. Moreover, when Cu^{2+} was used to replace Ni^{2+} as the catalyst, the yield could be further increased to 65.2 ± 3.2 g NH_3/t olivine (Figure S2). When no catalyst was added, the amount of NH_3 produced by the reaction between the olivine and the nitrate solution was 20.5 ± 4.0 g NH_3/t olivine (Figure S3). These findings conclusively prove the concept of producing NH_3 through subsurface rock-nitrate aqueous solution reactions, showcasing a novel pathway for Geo-NH_3 generation.

Figure 2E shows a relatively high NH_3 yield when using Cu^{2+} as a catalyst under ambient conditions, with a 35% higher yield than the Ni^{2+} catalyst at 90°C and I atm. Moreover, this yield was, surprisingly, achieved in just 10 min, indicating the fast kinetics of this reaction and suggesting that geological NH_3 may be significantly easier to produce than Geo-H_2. To further confirm that the NH_3 production was indeed from the reaction between the simulated mineral $Fe(OH)_2$ and aqueous $NaNO_3$, a series of controlled (Figure S4) and isotopic experiments (Figure 2F) were carried out. In the absence of catalysts, $Fe(OH)_2$ and $NaNO_3$ can also react to produce NH_3 but the yield drops by half (Figure S4A). In the absence of nitrate, no NH_3 was produced, as expected (Figure S4B). Further controlled experiments ruled out the possibility of NH_3 coming from $Fe(OH)_2$ (Figure S4C), $NaNO_3$ (Figure S4D), or $CuCl_2$ (Figure S4E) alone, respectively. NH_3 cannot be produced when there is no ferrous iron in the system either (Figure S4F), which demonstrates that ferrous iron acts as the reducing agent in the NH_3 formation reaction. Furthermore, we performed isotopic measurements (Figure 2F), confirming that the NH_3 is indeed generated through the Geo-NH_3 reaction (Equation 5) from the provided N-source (^{14}N or ^{15}N) and is not from impurity. Overall, the systematic controlled experiments rule out the possibility of false-positive NH_3 production from impurities and side reactions (Figures S4B–S4F, 2E, and 2F, Table S1, and Note S3).

We further investigated the Geo-NH_3 production from different nitrate concentrations. As shown in Figure 2G, Geo-NH_3 can be produced from nitrate solutions of varying concentrations from 25 to 0.83 mM. These nitrate concentrations are comparable with those found in industrial wastewater (41.6 mM), textile wastewater (7.4 mM), and polluted ground water (0.88–1.26 mM).[13] When the nitrate concentration is reduced from 25 mM (comparable with industrial wastewater) to 1.67 mM (comparable with polluted ground water), the amount of Geo-NH_3 produced is decreased by only 8%, with 9.6 kg NH_3/t $Fe(OH)_2$ produced. Therefore, Geo-NH_3 can be produced from nitrate-containing wastewater as a feedstock. This strongly demonstrates the competitive advantage of our method compared with other NH_3 production methods from nitrate, e.g., electrocatalytic reduction, which requires nitrate concentrations (typically 30–100 mM)[13] and solution conductivity (typically 500 mM $NaSO_4$)[13] that are too high when compared with wastewater. When considering the NH_3 cycle in industrial systems, NH_3 is mostly produced as industrial chemicals or fertilizers and is eventually converted or naturally converted to NO_3^- in the form of industrial wastewater, agricultural runoff, etc. By repurposing industrial waste, our method provides the dual benefits of NH_3 production and waste disposal revenue, enhancing sustainability and lowering the production costs of Geo-NH_3, similar to the advantage of using wastewater for green-NH_3.[13,14,18–21,40]

Furthermore, the amount of NH_3 produced per tonne of olivine is promising for scalability. We generated 1,752.6 ± 96.9 g NH_3/t of olivine at 300°C with Cu^{2+} as a catalyst in just 21 h (Figure 2H). This result is approximately 30 times the amount at 130°C (65.2 ± 3.2 g NH_3/t of olivine) and represents a significant improvement compared with previous reports, where only trace amounts of NH_3 were observed after several days.[25–28] The reaction time could be further optimized to improve efficiency. Additionally, if we scale up this technology, a typical two-borehole system could access approximately 25 million tonne of olivine, which, in principle, could produce around 40,000 t of NH_3 per commercial well.[41–43] With full-scale production, a multi-borehole system adapted from the oil and gas industry would increase the production rate by additional orders of magnitude.

Oxidation of rock during geological ammonia generation

As mentioned earlier, "Geo-NH_3" has been produced by a novel modified serpentinization reaction by the oxidation of Fe^{2+} in minerals (both olivine and synthetic) to Fe^{3+} (to form Fe_3O_4). In order to probe and further support the above-mentioned strategy for NH_3 generation, the X-ray diffraction (XRD) of olivine and synthetic minerals before and after the reaction has been recorded with a Mo Kα energy source. The synthetic mineral is present in the $Fe(OH)_2$ phase (without any notable impurity peaks), as examined by XRD (Figure 3A), meaning that Fe is in its +2-oxidation state. After the NH_3 generation reaction, Fe^{2+} in the synthetic mineral gets oxidized to Fe^{3+} and forms Fe_3O_4. XRD of the synthetic mineral (Figure 3B) shows its transformation from $Fe(OH)_2$ (before reaction) to Fe_3O_4 (after reaction). This means that some of the Fe was oxidized to the +3-oxidation state.

In addition to the synthetic mineral, the olivine (Figure S5) also shows its partial transformation from the $(Mg,Fe)_2SiO_4$ phase

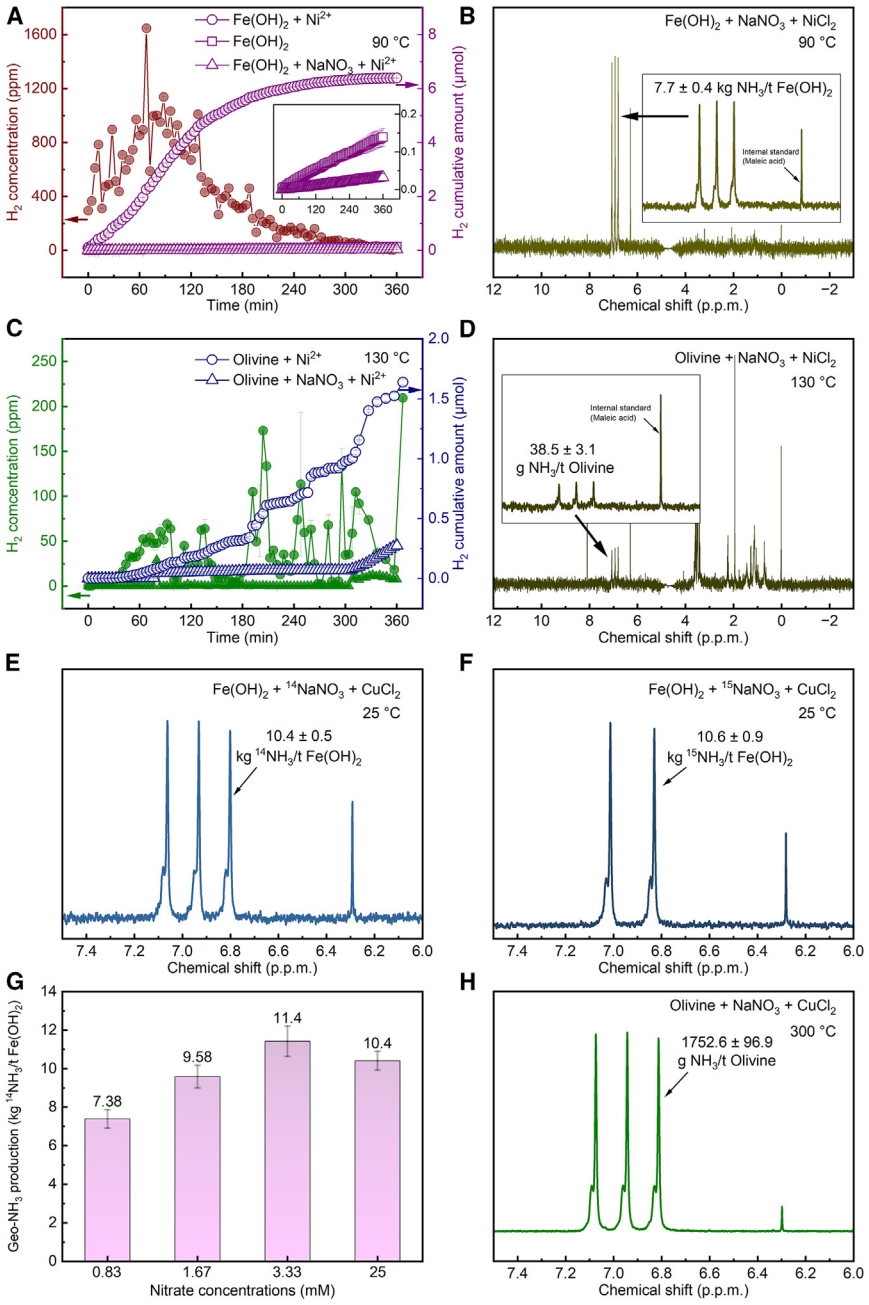

Figure 2. Generation of H_2 and NH_3 from rock

(A) Gas chromatography of H_2 generation during the reaction between the synthetic mineral ($Fe(OH)_2$) of rock and fluid at 90°C, 0.1 MPa, and pH∼7. Although the rate and yield are very low without a catalyst (black), adding 1 wt % of Ni catalyst enhances the rate and yield by 50× (red). However, almost no H_2 generation is observed in the presence of nitrate, even with a catalyst (magenta).

(B) NH_3 is instead generated after 6 h reaction, confirmed by nuclear magnetic resonance (NMR).

(C) H_2 generation from the actual mineral (olivine), using Ni as catalyst (blue) at 130°C, 0.25 MPa. There is 10× enhancement in rate and yield compared with previous reports without a catalyst. Very low H_2 generation was observed in the presence of nitrate, even with a catalyst (magenta).

(D) NMR confirmation of NH_3 generation from olivine after 21 h reaction.

(E) Using Cu^{2+} as a catalyst, large amounts of Geo-NH_3 can be produced in just 10 min under ambient conditions (i.e., room temperature and pressure).

(F) Isotopic measurement of $^{15}NH_3$ formation using $^{15}NO_3^-$ sources in 10 min under ambient conditions. The formation of respective isotopic ammonia (triplet and doublet peaks) proves that quantified ammonia is a direct product of geological reaction (not impurity).

(G) Amounts of Geo-NH_3 production from different nitrates concentration in 10 min under ambient conditions.

(H) Geo-NH_3 production from olivine at 300°C and 8.5 MPa after 21 h reaction. Nitrate concentration not otherwise specified is 25 mM.

The error bars represent the standard deviation.

(before reaction), possibly on the surface to Fe_3O_4 (Figure S6), as observed from XRD results, confirming the oxidation of the mineral after the NH_3 generation reaction. The phase fractions of different phases present in the rock samples before and after the reaction were also estimated by Rietvelt refinement of XRD patterns (Figures S7 and S8). It is found that the rock samples before reaction possess 80.5% olivine phase (suggesting the rock before reaction consists of majority of olivine phase) and the rest other impurity phases mentioned in Figure S7. Interestingly, after the reaction, the impurity phases rich in alkali metal ions (such as Ca^{2+}-containing impurities) are not present in the XRD. This absence could be due to dissolution in the alkaline solution of the reaction mixture, a phenomenon commonly reported in such reactions.[44–46] Additionally, some of the olivine phase converted to Fe_3O_4 after the reaction (Figure S8), clearly suggesting Fe^{2+} oxidation to Fe^{3+} in the olivine phase.

To re-confirm the same and accurately probe the oxidation state of the Fe in synthetic minerals before and after the reaction, X-ray photoelectron spectroscopy (XPS) was conducted before and after the reaction, as shown in Figures 3C and 3D, respectively. In support of the XRD results, XPS also shows that oxidation of Fe (from Fe^{2+} before the reaction; see Figure 3C) has clearly taken place during the serpentinization reaction to +3 oxidation (to form Fe_3O_4 after the reaction; see Figure 3D). Besides, the scanning electron microscope (SEM)-energy dispersive spectrometer (EDS) images show the co-existence of Fe with Ni or Cu in the reacted rock samples (Figure S9). The by-products of this reaction, including magnetite and others, are minerals. Thus, in principle, the ore left behind after the *in situ*

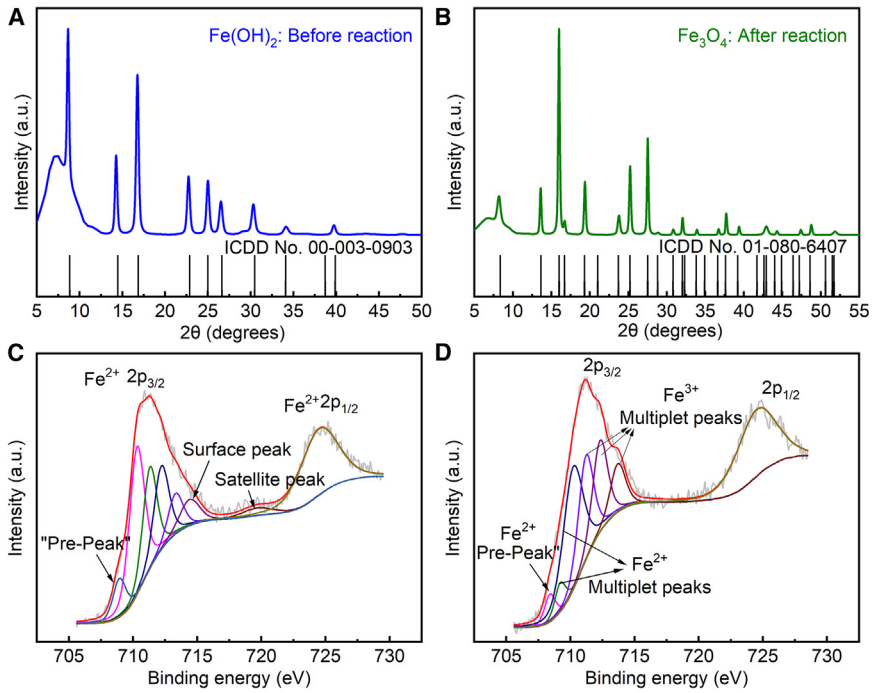

Figure 3. Chemical and structural transformation of synthetic mineral samples

(A) $Fe(OH)_2$ was transformed to (B) Fe_3O_4 (magnetite), which was confirmed by X-ray diffraction. X-ray photoemission spectroscopy before and after the reaction confirmed the oxidation of Fe^{2+} in $Fe(OH)_2$ (C) to Fe^{3+} in magnetite (D).

production of ammonia can still remain in the ground, which can be mined for iron ore if necessary or used for CO_2 sequestration.[47–49] Other potentially harmful byproducts are to be investigated in further field tests.

Reaction mechanism and techno-economic outlook

Figure S10 shows that no NH_3 was generated from the reaction mixture of nitrate and base, wherein H_2 was constantly purged. This indicates that our Geo-NH_3 generation from ferrous hydroxide and nitrate is unlikely to involve H_2 evolution for nitrate reduction. Given that NH_3 was produced from a basic aqueous mixture of $Fe(OH)_2$ and $NaNO_3$, even without metal ion catalysts (Figure S4A), the Geo-NH_3 generation can be considered a direct nitrate reduction by $Fe(OH)_2$, which leaves Fe_3O_4 as the oxidized product. Below are the half-reactions in basic condition:

$$3\,Fe(OH)_2\,(s) + 2\,OH^-\,(aq) \rightarrow Fe_3O_4\,(s) + 4\,H_2O\,(l) + 2\,e^- \quad \text{(Equation 6)}$$

$$NO_3^-\,(aq) + 6\,H_2O\,(l) + 8\,e^- \rightarrow NH_3\,(l) + 9\,OH^-\,(aq) \quad \text{(Equation 7)}$$

As mentioned above, the reaction can be promoted by the addition of metal ions (i.e., Ni^{2+} or Cu^{2+}). A similar phenomenon was reported by Song et al. for the low-temperature serpentinization,[33] where Ni^{2+} boosted the H_2 production by forming coprecipitation with $Fe(OH)_2$ in basic media. Their computational result indicated that the Ni^{2+}-coprecipitated $Fe(OH)_2$ exhibits higher electron density on Ni sites and stronger adsorption-free energy for H_2O on both Ni and Fe sites than those of pure $Fe(OH)_2$. Similarly, we speculate that Ni^{2+} or Cu^{2+}, which has low K_{sp} values of 5.48×10^{-16} ($Ni(OH)_2$) and 2.20×10^{-20} ($Cu(OH)_2$),[50] forms coprecipitation with $Fe(OH)_2$, presumably providing for an enhanced affinity of nitrate onto the surface as well as higher electron density for promoting the subsequent reduction reaction.

Furthermore, we investigated the reaction (Equation 5) mechanism to explain our experimental results and suggest a potential reaction pathway by density functional theory (DFT) calculations. For the reaction in Equation 5, the hydrogen sources in NH_3 is either from H_2O or $Fe(OH)_2$. First, we consider $Fe(OH)_2$ as the hydrogen source. When a NO_3^- ion adsorbs on the surface, it reacts with surface OH^- to generate HNO_3*, as shown in Figures 4A and 4B below. In Figure 4A, the structure of HNO_3*, generated from NO_3* and the nearest surface OH^- (indicated by the arrow), has a ΔG of 1.77 eV. This structure is HNO_4*, a stable tetrahedron unit, making it unfavorable for subsequent reactions. In Figure 4B, the structure of HNO_3* formed with the second-nearest surface OH^- (indicated by the arrow) has a ΔG of 2.62 eV, which is too high. Finally, we consider the hydrogen originating from H_2O. The adsorbed H_2O reacts with the adsorbed NO_3*, producing HNO_3* and OH*, as depicted in Figure 4C. This reaction has a ΔG of 1.66 eV, making it energetically more favorable than the previous two scenarios, with energy differences of ~40 and ~$4K_bT$ compared to Figures 4A and 4B, respectively). Based on these observations, we conclude that the hydrogen in NH_3 comes from H_2O rather than $Fe(OH)_2$. Therefore, in the following calculations, we will consider H_2O as the hydrogen source for NH_3 (as shown in Equation 8):

$$12Fe(OH)_2 + 6H_2O + XNO_3 \rightarrow NH_3 + 4Fe_3O_4 + 16H_2O + XOH\ (X{=}Na, K, etc.) \quad \text{(Equation 8)}$$

Our experimental results in Figure 2 suggest that catalysts/additives such as Ni can enhance both the rate and yield of NH_3 generation. To understand the mechanism behind this, we performed DFT calculations to study NH_3 generation on the (100) surface of $Fe(OH)_2$ and Ni-doped $Fe(OH)_2$. Figure 4D shows the calculated free energy changes along the reaction pathway, with the structures of each intermediate on the Ni-doped $Fe(OH)_2$ surface depicted shown in Figure S11. It is evident that Ni-doped $Fe(OH)_2$ exhibits stronger adsorption energy for NO_3^- (−2.54 eV on Ni-doped $Fe(OH)_2$ and −1.69 eV on $Fe(OH)_2$), which is beneficial for the subsequent reactions (see more details on Note S4). Moreover, the overall free energy changes on Ni-doped $Fe(OH)_2$ are more negative, indicating a thermodynamically more favorable process.

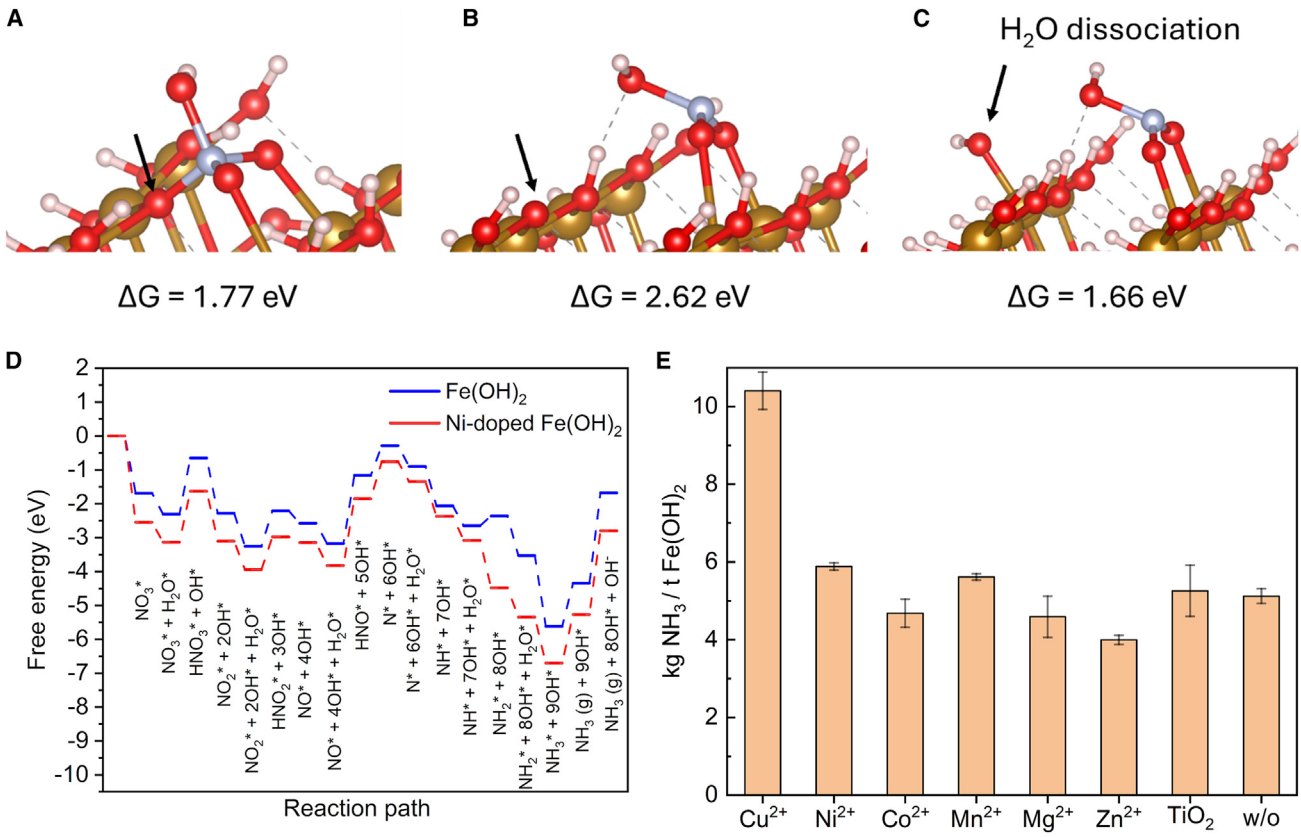

Figure 4. Reaction mechanism investigation and catalyst optimization

(A and B) HNO_3* generated from surface OH^- in $Fe(OH)_2$; (C) HNO_3* generated from surface H_2O (brown: Fe; light blue: N; red: O; white: H).

(D) Free energy diagram of the NH_3 generation on $Fe(OH)_2$ and Ni-doped $Fe(OH)_2$ (100) surface, where the H in NH_3 is from water.

(E) Comparative experimental analysis of various catalysts on the amount of Geo-NH_3 produced. Except for the catalyst type, all reaction conditions were kept the same under ambient conditions (i.e., room temperature and pressure in 10 min). The error bars represent the standard deviation.

In addition, we investigated the effect of different additives on the amount of Geo-NH_3 produced by experiments (Figure 4E). Copper ion (Cu^{2+}), nickel ion (Ni^{2+}), and manganese (Mn^{2+}) all favored Geo-NH_3 production, with copper ion being the most effective. TiO_2 suspended particles, cobalt (Co^{2+}), and magnesium (Mg^{2+}) ions have little effect on NH_3 production, whereas zinc ion (Zn^{2+}), by contrast, reduced NH_3 production compared with no addition (w/o). This result helps provide guidance for the addition of catalysts to aqueous solutions pumped underground to further enhance the rate of Geo-NH_3 production. Meanwhile, it is worth noting that there are some rocks containing these catalysts naturally (already identified in Costa Rica, Oregon, and California[51]). Therefore, the co-existence of such elements with rocks needs to be considered when exploring sites for Geo-NH_3 extraction.

Finally, we performed a preliminary techno-economic outlook of Geo-NH_3. We first estimated the amount of Geo-NH_3 reserves in the Earth that can be produced from rocks. According to research reports on Geo-H_2, a back-of-the-envelope calculation for the first 7 km of the Earth's crust estimates that there is enough Fe^{2+} to produce H_2 for 250,000 years (100 trillion tonnes of H_2 at a rate of 400 Mt annually).[52–54] Accordingly, we can calculate that the Earth could produce sufficient NH_3 for 2,420,000 years, with 570 trillion tonnes of NH_3 at a rate of 235 Mt annually. Then, we performed a cost assessment of the Geo-NH_3 production process (Figure S12; Table S2). The cost of capital expenditures, such as borehole drilling and rock cracking, and operational expenditures, such as nitrate source, water, and catalyst, etc., were considered. The cost of NH_3 is estimated to be \$0.55 per kg of NH_3 with NO_3^- as the nitrogen source (Table S2). The cost can be further reduced to \$0.46 per kg NH_3 if the Geo-NH_3 reaction is performed on ultramafic rock formations naturally containing Ni or Cu catalysts.[51] The use of N-source with natural catalysts brings the cost of Geo-NH_3 close to cost parity with the gray-NH_3 (Haber-Bosch, \$0.4/kg NH_3[40,55]), blue-NH_3 (Haber-Bosch with CO_2 sequestration, \$0.8/kg NH_3), and turquoise-NH_3 (Pyrolysis + Haber-Bosch process, \$0.8/kg NH_3) and is cheaper than NH_3 production using electrolyzers (\$2.17/kg NH_3[14,15]). Moreover, integrating NO_3^- wastewater treatment with NH_3 co-production could yield an additional profit of \$3.82/kg of NH_3,[14] potentially improving the economic viability of our process.

Furthermore, if N_2 is used as a nitrogen source, the cost is estimated to be \$0.3–\$0.5/kg NH_3, making the Geo-NH_3 an ideal pathway at scale. In addition, the environmental advantages of this method are substantial. In contrast with the Haber-Bosch (which emits 3 kg CO_2/kg NH_3 from the use of black H_2 and

maintaining temperatures and pressures for reactions[40,55]), the CO_2 footprint from our method is minimal. Although some energy usage and resulting CO_2 emissions are unavoidable during the digging of wells and the transfer, collection, and NH_3 purification phases, they are anticipated to be no more than 0.1 kg CO_2/kg NH_3. See Note S5 for more details on the techno-economic outlook. We made the first attempt to perform techno-economic analysis on this new technology, and more in-depth studies are needed in the future. Beyond *in situ* reactions, our method is also applicable to *ex situ* setups where mined Fe^{2+}-containing rocks, such as iron ore tailings, are used to produce Geo-NH_3 in above-ground reactors (Figure S13). This flexibility in application further supports the practicality and scalability of our method. Moreover, there are a growing number of techniques that are attempting to produce nitrate directly from N_2 bypassing NH_3, including plasma oxidation,[56,57] electrocatalytic oxidation,[58,59] ultrasound H_2O_2,[60] and many other methods.[61] We believe that these strategies for the direct production of nitrate from N_2 offer the possibility of sustainable production of nitrate and further sustainable production of Geo-NH_3.

In summary, our approach demonstrated that NH_3 can be efficiently generated from rocks with nitrate-source water at 130°C (65.2 ± 3.2 g NH_3/t olivine), 300°C (1,752.6 ± 96.9 g NH_3/t olivine), and even at ambient temperature and pressure (10.4 ± 0.5 kg NH_3/t $Fe(OH)_2$). Our method for Geo-NH_3 production, involving only the injection of nitrate-source water into the subsurface to utilize *in situ* subsurface thermal and pressure, requires no external H_2 and emits no CO_2. Through experimental investigations and theoretical calculations, we have identified, for the first time, the fundamental chemical process enabling stimulated Geo-NH_3 production, where the Fe^{2+} naturally present in rocks reduces nitrate to form NH_3, and the hydrogen in NH_3 comes from H_2O rather than the mineral. Our work establishes a foundation for utilizing Earth's subsurface as a natural reactor, leveraging abundant rocks, subsurface heat, and pressure as resources to produce sufficient NH_3 for 2,420,000 years with 570 trillion tonnes of NH_3 at a rate of 235 Mt annually, with minimal environmental impacts and in an economically feasible manner, thereby achieving sustainability and decarbonization of the chemical and energy sectors. Future work, such as converting CO_2 to valuable chemicals by injecting it into the subsurface, as well as systematic assessment of the environmental footprint of Geo-H_2/NH_3/CO_2 sequestration technologies, would be impactful. Understanding the complex interface between rocks and reacting fluid is a rich area to explore, achieved by combining advanced computational and experimental methods to push our knowledge in this field. Additionally, at the system level, engineering designs to implement what is proposed in this work in the real world represent fertile ground for new concepts and methods at the intersection of the chemical, mining, and oil and gas industries.

RESOURCE AVAILABILITY

Lead contact

Further information and requests for resources should be directed to and will be fulfilled by the lead contact, Iwnetim I. Abate (iabate@mit.edu).

Materials availability

This study did not generate new, unique materials.

Data and code availability

The data generated in this study are provided in the paper and supplemental information. This study did not generate code. Additional relevant data are available from the corresponding author on request.

METHODS

Materials

Olivine was purchased from Ward's Science. Chemicals including sodium nitrate (99.995% trace metals basis), sodium nitrate-^{15}N (≥98 atom % ^{15}N), iron (II) chloride (99.99% trace metals basis), copper(II) chloride (97%), nickel(II) chloride hexahydrate (99.999% trace metals basis), sodium hydroxide (anhydrous, ACS reagent), sulfuric acid (99.999%), maleic acid (standard for quantitative NMR), and deuterium oxide (≥99.95 atom % D) were purchased from Sigma-Aldrich without further purification. Deoxygenated deionized water was flushed with argon for 30 min to remove dissolved oxygen and stored in a glove box that was oxygen free (O_2 concentration < 0.5 ppm) but allowed aqueous solution, referred to as "water glove box" for short in the following.

Geological NH_3 or H_2 production experimental setup

The rock-water reaction system, as shown in Figure S1, includes an autoclave reactor integrated with a gas system and a heating system (Figure S1A). The autoclave reactor is equipped with a gas inlet and a gas outlet, where both inlet and outlet pipelines are fitted with gas mass flow controllers to control and record the gas flow. The gas inlet can be connected to an argon gas cylinder to supply argon as a carrier gas. Additionally, the gas outlet can be linked to a gas chromatograph (GC) for real-time *in situ* measurement of the gas composition and concentration inside the autoclave. The heating system is capable of controlling and measuring the internal temperature of the autoclave reactor. A temperature probe is inserted tunnel-like into the interior of the autoclave. Based on the temperature feedback from the temperature probe and the set target temperature, the heating base adjusts to regulate the temperature.

For actual mineral reaction experiments, olivine minerals were processed through crushing with a hammer, coarse grinding, and fine grinding until powdered samples were obtained for subsequent experiments. Within an argon-gas-filled water glove box, a certain amount of olivine powder, deoxygenated deionized water, $NaNO_3$ solution, NaOH solution, and a solution of $CuCl_2$ or $NiCl_2$ as a catalyst are sequentially added into the autoclave (Figure S1B) and then sealed. For simulated mineral reaction experiments, a certain amount of $FeCl_2$ solution, NaOH solution, a solution of $CuCl_2$ or $NiCl_2$ as a catalyst, and $NaNO_3$, are sequentially introduced into the autoclave and sealed. In this case, the first added chemicals, $FeCl_2$ and NaOH, would *in situ* produce $Fe(OH)_2$ precipitate, which was used as a simulated mineral. The autoclave is then placed within the heating system and connected to the gas pipeline system (Figure S1C), after which the temperature and operation duration are set to start the experiment. For Geo-H_2 experiments, $NaNO_3$ was not added; instead, an equivalent volume of deionized water is used to ensure the overall reaction volume and the concentrations of other reactants remain unchanged. For rapid tube tests at room temperature, neither the high-pressure autoclave reactor nor the heating system is required; the simulated

rock-water reaction was simply completed within a test tube. These rapid tube tests were performed for optimization and mechanism investigation, so we chose to react for 10 min to improve efficiency, whereas for the actual olivine mineral we chose to react for 21 h to explore NH_3-producing capacity. The isotopic experiment was conducted by using ^{15}N-$NaNO_3$ instead of ^{14}N-$NaNO_3$ as a reactant in similar experimental conditions.

Characterizations

Solid samples after experiments were obtained by separating solid and liquid through a vacuum filtration system set up in the water glove box. Powder X-ray diffraction (Panalytical Empyrean, Mo K-α radiation, $\lambda = 0.7107$ Å) was used to determine the crystal structure of the model compounds and minerals before and after the reaction. X-ray photoelectron spectroscopy (XPS; PHI VersaProbe II X-ray Photoelectron Spectrometer) was performed, using monochromated Al K-alpha (X-radiation pass energy = 2.95 eV) as the excitation source, to look into the oxidation states of the Fe close to the surface of the particles. In all the characterization techniques used above, to capture the accurate data before and after the reaction, samples were protected while doing all the characterizations by using air-free holders.

NH_3 and H_2 production rate measurements and calculations

The NH_3 concentration in solution was measured directly via nuclear magnetic resonance[62] (NMR). All tests were repeated at least three times. A certain amount of maleic acid (MA) was added as an internal standard, as well as a certain amount of H_2SO_4 to adjust the pH to the solution after filtration. 1H NMR spectra were obtained using a three-channel Bruker Avance Neo spectrometer operating at 400.17 MHz. A standard curve is established based on the internal MA and external NH_4Cl standards. For all the NMR results, we have quantitatively calculated NH_3 concentration based on the standard chemical (MA as internal standard). The NH_3 yield (g NH_3/t olivine or g NH_3/kgFe^{2+}) can be converted from the solution NH_3 concentration and the mass of rock added at the beginning of the reaction. The NH_3 production ratio was obtained by dividing the actual NH_3 production by the theoretical maximum by production when oxidizing all Fe^{2+} in the rock to Fe_3O_4.

The composition and concentration of the gas in the autoclave were analyzed *in situ* by a GC (MG#5, SRI) equipped with a high-sensitivity thermal conductivity (TCD) detector[33] directly connected to the outlet of the autoclave. A standard curve is established based on the external H_2 standards, and the H_2 concentration in the gas can be calculated. The H_2 yield (μmol g^{-1} h^{-1}) can be converted from the outlet gas H_2 concentration, total volume of the autoclave system, and the mass of rock added at the beginning of the reaction. The H_2 production ratio was obtained by dividing the actual H_2 production by the theoretical maximum by production when oxidizing all Fe^{2+} in the rock to Fe_3O_4.

DFT calculation method

We carried out spin-polarized DFT calculations using the Vienna *ab initio* simulation package (VASP5.4.4).[63] The Generalized Gradient Approximation (GGA) of Perdew, Burke, and Ernzerhof (PBE)[64] was used to model electron exchange-correlation interactions, employing a plane waves cutoff of 400 eV. We employed Grimme's DFT + D3 method[65] to account for the van der Waals interactions. The Hubbard U correction (DFT+U) was incorporated to accurately describe the correlation energy for the 3d orbitals of Fe and Ni atoms, using effective parameters U-J of 5.67 and 5.23 eV for Fe and Ni, respectively, as referenced from Song et al.[33] The convergence criteria for energy and force were set at 10^{-5} eV and 0.03 eV·Å^{-1}, respectively. A 2 × 2 × 1 Monkhorst-Pack grid was used to sample the electron's Brillouin zone.

We constructed a 4 × 3 supercell with two layers of the (100) surface of $Fe(OH)_2$. For the Ni-doped $Fe(OH)_2$ scenario, one surface Fe atom was replaced with Ni. During structural relaxation, the bottom layer remained fixed, whereas the top layer was allowed to relax. We tested the H_2O adsorption energy on the constructed surface, confirming that the chosen supercell size and layers were sufficient for the convergence of H_2O adsorption energy. The adsorption energy was computed as follows:

$$E_{ads} = E_{(slab+adsorbate)} - (E_{slab} + E_{adsorbate})$$

We considered the zero-point energy (ZPE) and entropy correction to the adsorbates. We used VESTA for the structure visualization.[66]

ACKNOWLEDGMENTS

The authors would like to thank Zhen Zhang for the design of the reactor used in this work and Hongbin Xu for support with the initial NMR experiments. This work was supported by the MIT Climate Grand Challenges. This work was carried out, in part, through the use of MIT.nano's facilities, supported by the National Science Foundation under award ECCS-1542152, and the Department of Chemistry Instrumentation Facility, supported by the National Science Foundation under awards HE-9808061 and DBI-972959. The computational work used Expanse at San Diego Supercomputer Center through allocation MAT230005 from the Advanced Cyberinfrastructure Coordination Ecosystem: Services & Support (ACCESS) program, which is supported by National Science Foundation grants #2138259, #2138286, #2138307, #2137603, and #2138296.

AUTHOR CONTRIBUTIONS

I.I.A. conceived the project; I.A.A. and J.L. supervised the experiments; Y.G. synthesized the materials, performed all reactions and GC and NMR measurements, and analyzed the data; B.S.K. and H.B.S. performed XRD and XPS measurements and analyzed the data; Y.G. and L.S. prepared the rock samples and performed reactions; Y.G. and S.H.H. developed the mechanism and performed controlled experiments; I.I.A. supervised the DFT calculations; M.L. performed DFT calculations; all authors contributed to interpreting the data; Y.G., B.S.K., S.H.H., and I.I.A. wrote the manuscript with input from all authors; I.I.A. directed the overall research.

DECLARATION OF INTERESTS

I.I.A., J.L. and Y.G. are inventors on patent applications related to the subject of this manuscript filed by the Massachusetts Institute of Technology. I.I.A. is the founder and a shareholder of Addis Energy, a company focused on the commercialization of the technology described in this study. The company had no role in the study design, data collection, data analysis, decision to publish, funding, or preparation of the manuscript.

SUPPLEMENTAL INFORMATION

Supplemental information can be found online at https://doi.org/10.1016/j.joule.2024.12.006.

Received: August 12, 2024
Revised: October 31, 2024
Accepted: December 10, 2024
Published: January 21, 2025

REFERENCES

1. The International Energy Agency. New IEA study examines the future of the ammonia industry amid efforts to reach net zero emissions. https://www.iea.org/news/new-iea-study-examines-the-future-of-the-ammonia-industry-amid-efforts-to-reach-net-zero-emissions.
2. Ornes, S. (2021). Core Concept: Green ammonia could produce climate-friendly ways to store energy and fertilize farms. Proc. Natl. Acad. Sci. USA *118*, e2119584118. https://doi.org/10.1073/pnas.2119584118.
3. Robert, F., Service Ammonia—a renewable fuel made from sun, air, and water—could power the globe without carbon. https://www.science.org/content/article/ammonia-renewable-fuel-made-sun-air-and-water-could-power-globe-without-carbon.
4. Joseph Sekhar, S., Samuel, M.S., Glivin, G., Le, T., and Mathimani, T. (2024). Production and utilization of green ammonia for decarbonizing the energy sector with a discrete focus on Sustainable Development Goals and environmental impact and technical hurdles. Fuel *360*, 130626. https://doi.org/10.1016/j.fuel.2023.130626.
5. Al-Aboosi, F.Y., El-Halwagi, M.M., Moore, M., and Nielsen, R.B. (2021). Renewable ammonia as an alternative fuel for the shipping industry. Curr. Opin. Chem. Eng. *31*, 100670. https://doi.org/10.1016/j.coche.2021.100670.
6. Ammonia Energy Association. Zero Emission Aircraft: Ammonia for Aviation. https://ammoniaenergy.org/articles/zero-emission-aircraft-ammonia-for-aviation/.
7. Spatolisano, E., Pellegrini, L.A., de Angelis, A.R., Cattaneo, S., and Roccaro, E. (2023). Ammonia as a Carbon-Free Energy Carrier: NH3 Cracking to H2. Ind. Eng. Chem. Res. *62*, 10813–10827. https://doi.org/10.1021/acs.iecr.3c01419.
8. Rouwenhorst, K.H.R., Travis, A.S., and Lefferts, L. (2022). 1921–2021: A Century of Renewable Ammonia Synthesis. Sustain. Chem. *3*, 149–171. https://doi.org/10.3390/suschem3020011.
9. DECHEMA e.V. (2022). Carbon Dioxide Emissions from Ammonia Production in Europe Could Be Cut by Almost a Fifth in 2030. https://dechema.de/en/10_22_e.html.
10. The International Energy Agency. Executive Summary – Ammonia Technology Roadmap – Analysis. https://www.iea.org/reports/ammonia-technology-roadmap/executive-summary.
11. Osselin, F., Soulaine, C., Fauguerolles, C., Gaucher, E.C., Scaillet, B., and Pichavant, M. (2022). Orange hydrogen is the new green. Nat. Geosci. *15*, 765–769. https://doi.org/10.1038/s41561-022-01043-9.
12. Fu, X., Pedersen, J.B., Zhou, Y., Saccoccio, M., Li, S., Sažinas, R., Li, K., Andersen, S.Z., Xu, A., Deissler, N.H., et al. (2023). Continuous-flow electrosynthesis of ammonia by nitrogen reduction and hydrogen oxidation. Science *379*, 707–712. https://doi.org/10.1126/science.adf4403.
13. van Langevelde, P.H., Katsounaros, I., and Koper, M.T.M. (2021). Electrocatalytic Nitrate Reduction for Sustainable Ammonia Production. Joule *5*, 290–294. https://doi.org/10.1016/j.joule.2020.12.025.
14. Chen, F.-Y., Elgazzar, A., Pecaut, S., Qiu, C., Feng, Y., Ashokkumar, S., Yu, Z., Sellers, C., Hao, S., Zhu, P., et al. (2024). Electrochemical nitrate reduction to ammonia with cation shuttling in a solid electrolyte reactor. Nat. Catal. *7*, 1032–1043. https://doi.org/10.1038/s41929-024-01200-w.
15. Han, S., Li, H., Li, T., Chen, F., Yang, R., Yu, Y., and Zhang, B. (2023). Ultralow overpotential nitrate reduction to ammonia via a three-step relay mechanism. Nat. Catal. *6*, 402–414. https://doi.org/10.1038/s41929-023-00951-2.
16. Ferkov, A. Unpacking Ammonia's Market Landscape and Its Role in the Energy Transition. https://www.spglobal.com/commodityinsights/en/market-insights/blogs/energy-transition/091622-ammonia-prices-supply-demand-hydrogen-power-bunker-fuel.
17. Greenwald, J.E., Zhao, M., and Wicks, D.A. (2024). Critical mineral demands may limit scaling of green hydrogen production. Front. Geochem. *1*, 1328384. https://doi.org/10.3389/fgeoc.2023.1328384.
18. Chen, Y., Ammari-Azar, P., Liu, H., Lee, J., Xi, Y., Castellano, M.J., Gu, S., and Li, W. (2023). Sustainable waste-nitrogen upcycling enabled by low-concentration nitrate electrodialysis and high-performance ammonia electrosynthesis. EES. Catal. *1*, 504–515. https://doi.org/10.1039/D3EY00058C.
19. Wang, K., Mao, R., Liu, R., Zhang, J., Zhao, H., Ran, W., and Zhao, X. (2023). Intentional corrosion-induced reconstruction of defective NiFe layered double hydroxide boosts electrocatalytic nitrate reduction to ammonia. Nat Water *1*, 1068–1078. https://doi.org/10.1038/s44221-023-00169-3.
20. Guo, J., Liu, M.J., Laguna, C., Miller, D.M., Williams, K.S., Clark, B.D., Muñoz, C., Blair, S.J., Nielander, A.C., Jaramillo, T.F., et al. (2024). Electrodialysis and nitrate reduction (EDNR) to enable distributed ammonia manufacturing from wastewaters. Energy Environ. Sci. *17*, 8787–8800. https://doi.org/10.1039/D4EE03002H.
21. Miller, D.M., Liu, M.J., Abels, K., Kogler, A., Williams, K.S., and Tarpeh, W.A. (2024). Engineering a molecular electrocatalytic system for energy-efficient ammonia production from wastewater nitrate. Energy Environ. Sci. *17*, 5691–5705. https://doi.org/10.1039/D4EE01727G.
22. Klein, F., Bach, W., Jöns, N., McCollom, T., Moskowitz, B., and Berquó, T. (2009). Iron partitioning and hydrogen generation during serpentinization of abyssal peridotites from 15°N on the Mid-Atlantic Ridge. Geochim. Cosmochim. Acta *73*, 6868–6893. https://doi.org/10.1016/j.gca.2009.08.021.
23. Zgonnik, V. (2020). The occurrence and geoscience of natural hydrogen: A comprehensive review. Earth Sci. Rev. *203*, 103140. https://doi.org/10.1016/j.earscirev.2020.103140.
24. Czado, P.J.B., and Krystian. (2022). Natural hydrogen: the new frontier. Geoscientist. https://geoscientist.online/sections/unearthed/natural-hydrogen-the-new-frontier/.
25. Nishizawa, M., Saito, T., Makabe, A., Ueda, H., Saitoh, M., Shibuya, T., and Takai, K. (2021). Stable Abiotic Production of Ammonia from Nitrate in Komatiite-Hosted Hydrothermal Systems in the Hadean and Archean Oceans. Minerals *11*, 321. https://doi.org/10.3390/min11030321.
26. Shang, X., Huang, R., and Sun, W. (2023). Formation of ammonia through serpentinization in the Hadean Eon. Sci. Bull. *68*, 1109–1112. https://doi.org/10.1016/j.scib.2023.04.038.
27. Cheng, B., Hua, Y., Zhao, J., Liu, G., and Wan, X. (2020). Nitrogen transformation mediated by nitrate-dependent iron oxidation in anoxic freshwater. J. Soils Sediments *20*, 1087–1096. https://doi.org/10.1007/s11368-019-02461-w.
28. Smirnov, A., Hausner, D., Laffers, R., Strongin, D.R., and Schoonen, M.A.A. (2008). Abiotic ammonium formation in the presence of Ni-Fe metals and alloys and its implications for the Hadean nitrogen cycle. Geochem. Trans. *9*, 5. https://doi.org/10.1186/1467-4866-9-5.
29. Garibello, C.F., Eldridge, D.S., Malherbe, F., and Hocking, R.K. (2023). Abiotic transformations of nitrogen mediated by iron sulfides and related species from early Earth to catalyst design. Inorg. Chem. Front. *10*, 6792–6811. https://doi.org/10.1039/D3QI01553J.
30. Li, Y. (2024). The origin and evolution of Earth's nitrogen. Natl. Sci. Rev. *11*, nwae201. https://doi.org/10.1093/nsr/nwae201.
31. McGlynn, S.E., Glass, J.B., Johnson-Finn, K., Klein, F., Sanden, S.A., Schrenk, M.O., Ueno, Y., and Vitale-Brovarone, A. (2020). Hydrogenation reactions of carbon on Earth: linking methane, margarine, and life. Am. Mineral. *105*, 599–608. https://doi.org/10.2138/am-2020-6928CCBYNCND.
32. Dörr, M., Kässbohrer, J., Grunert, R., Kreisel, G., Brand, W.A., Werner, R.A., Geilmann, H., Apfel, C., Robl, C., and Weigand, W. (2003). A Possible Prebiotic Formation of Ammonia from Dinitrogen on Iron Sulfide Surfaces. Angew. Chem. Int. Ed. Engl. *42*, 1540–1543. https://doi.org/10.1002/anie.200250371.
33. Song, H., Ou, X., Han, B., Deng, H., Zhang, W., Tian, C., Cai, C., Lu, A., Lin, Z., and Chai, L. (2021). An Overlooked Natural Hydrogen Evolution Pathway: Ni2+ Boosting H2 O Reduction by Fe(OH)2 Oxidation during

Low-Temperature Serpentinization. Angew. Chem. Int. Ed. Engl. *60*, 24054–24058. https://doi.org/10.1002/anie.202110653.

34. Mayhew, L.E., Ellison, E.T., McCollom, T.M., Trainor, T.P., and Templeton, A.S. (2013). Hydrogen generation from low-temperature water–rock reactions. Nat. Geosci. *6*, 478–484. https://doi.org/10.1038/ngeo1825.
35. Klein, F., Bach, W., Humphris, S.E., Kahl, W.-A., Jöns, N., Moskowitz, B., and Berquó, T.S. (2014). Magnetite in seafloor serpentinite—Some like it hot. Geology *42*, 135–138. https://doi.org/10.1130/G35068.1.
36. Okland, I., Huang, S., Thorseth, I.H., and Pedersen, R.B. (2014). Formation of H2, CH4 and N-species during low-temperature experimental alteration of ultramafic rocks. Chem. Geol. *387*, 22–34. https://doi.org/10.1016/j.chemgeo.2014.08.003.
37. McCollom, T.M., and Bach, W. (2009). Thermodynamic constraints on hydrogen generation during serpentinization of ultramafic rocks. Geochim. Cosmochim. Acta *73*, 856–875. https://doi.org/10.1016/j.gca.2008.10.032.
38. Miller, H.M., Matter, J.M., Kelemen, P., Ellison, E.T., Conrad, M.E., Fierer, N., Ruchala, T., Tominaga, M., and Templeton, A.S. (2016). Modern water/rock reactions in Oman hyperalkaline peridotite aquifers and implications for microbial habitability. Geochim. Cosmochim. Acta *179*, 217–241. https://doi.org/10.1016/j.gca.2016.01.033.
39. McCollom, T.M., Klein, F., Moskowitz, B., Berquó, T.S., Bach, W., and Templeton, A.S. (2020). Hydrogen generation and iron partitioning during experimental serpentinization of an olivine–pyroxene mixture. Geochim. Cosmochim. Acta *282*, 55–75. https://doi.org/10.1016/j.gca.2020.05.016.
40. MacFarlane, D.R., Cherepanov, P.V., Choi, J., Suryanto, B.H.R., Hodgetts, R.Y., Bakker, J.M., Ferrero Vallana, F.M., and Simonov, A.N. (2020). A Roadmap to the Ammonia Economy. Joule *4*, 1186–1205. https://doi.org/10.1016/j.joule.2020.04.004.
41. Moore, R. The Numbers: The Permian Excels. https://www.pheasantenergy.com/the-numbers-the-permian-excels/.
42. The U.S. Energy Information Administration. Advances in technology led to record new well productivity in the Permian Basin in 2021. https://www.eia.gov/todayinenergy/detail.php?id=54079.
43. King, R.J. (2009). Olivine Group. Geol. Today *25*, 193–197. https://doi.org/10.1111/j.1365-2451.2009.00730.x.
44. Beglaryan, H., Isahakyan, A., Zulumyan, N., Melikyan, S., and Terzyan, A. (2023). A study of magnesium dissolution from serpentinites composed of different serpentine group minerals. Miner. Eng. *201*, 108171. https://doi.org/10.1016/j.mineng.2023.108171.
45. Portella, Y. de M., Conceição, R.V., Siqueira, T.A., Gomes, L.B., and Iglesias, R.S. (2024). Experimental evidence of pressure effects on spinel dissolution and peridotite serpentinization kinetics under shallow hydrothermal conditions. Geosci. Front. *15*, 101763. https://doi.org/10.1016/j.gsf.2023.101763.
46. Frost, B.R., and Beard, J.S. (2007). On Silica Activity and Serpentinization. J. Petrol. *48*, 1351–1368. https://doi.org/10.1093/petrology/egm021.
47. Matter, J.M., and Kelemen, P.B. (2009). Permanent storage of carbon dioxide in geological reservoirs by mineral carbonation. Nat. Geosci. *2*, 837–841. https://doi.org/10.1038/ngeo683.
48. Snæbjörnsdóttir, S.Ó., Sigfússon, B., Marieni, C., Goldberg, D., Gislason, S.R., and Oelkers, E.H. (2020). Carbon dioxide storage through mineral carbonation. Nat. Rev. Earth Environ. *1*, 90–102. https://doi.org/10.1038/s43017-019-0011-8.
49. Gíslason, S.R., Sigurdardóttir, H., Aradóttir, E.S., and Oelkers, E.H. (2018). A brief history of CarbFix: Challenges and victories of the project's pilot phase. Energy Procedia *146*, 103–114. https://doi.org/10.1016/j.egypro.2018.07.014.
50. Rumble, J.R., Lide, D.R., and Bruno, T.J. (2018). CRC Handbook of Chemistry and Physics: a Ready-Reference Book of Chemical and Physical Data, Ninty-Ninth Edition (CRC Press).
51. Schwarzenbach, E.M., Caddick, M.J., Beard, J.S., and Bodnar, R.J. (2016). Serpentinization, element transfer, and the progressive development of zoning in veins: evidence from a partially serpentinized harzburgite. Contrib. Mineral. Petrol. *171*, 5. https://doi.org/10.1007/s00410-015-1219-3.
52. Neal, C., and Stanger, G. (1983). Hydrogen generation from mantle source rocks in Oman. Earth Planet. Sci. Lett. *66*, 315–320. https://doi.org/10.1016/0012-821X(83)90144-9.
53. Kelemen, P.B., Matter, J., Streit, E.E., Rudge, J.F., Curry, W.B., and Blusztajn, J. (2011). Rates and Mechanisms of Mineral Carbonation in Peridotite: Natural Processes and Recipes for Enhanced, in situ CO2 Capture and Storage. Annu. Rev. Earth Planet. Sci. *39*, 545–576. https://doi.org/10.1146/annurev-earth-092010-152509.
54. Mao, H.-K., Hu, Q., Yang, L., Liu, J., Kim, D.Y., Meng, Y., Zhang, L., Prakapenka, V.B., Yang, W., and Mao, W.L. (2017). When water meets iron at Earth's core–mantle boundary. Natl. Sci. Rev. *4*, 870–878. https://doi.org/10.1093/nsr/nwx109.
55. Li, Y., Zhang, Z., Wang, Q., Long, X., Cao, Y., Yang, H., and Yang, Q. (2023). The nitrogen and carbon footprints of ammonia synthesis in China based on life cycle assessment. J. Environ. Manag. *345*, 118848. https://doi.org/10.1016/j.jenvman.2023.118848.
56. Kelly, S., and Bogaerts, A. (2021). Nitrogen fixation in an electrode-free microwave plasma. Joule *5*, 3006–3030. https://doi.org/10.1016/j.joule.2021.09.009.
57. Kong, X., Ni, J., Song, Z., Yang, Z., Zheng, J., Xu, Z., Qin, L., Li, H., Geng, Z., and Zeng, J. (2024). Synthesis of hydroxylamine from air and water via a plasma-electrochemical cascade pathway. Nat. Sustain. *7*, 652–660. https://doi.org/10.1038/s41893-024-01330-w.
58. Wang, Y., Li, T., Yu, Y., and Zhang, B. (2022). Electrochemical Synthesis of Nitric Acid from Nitrogen Oxidation. Angew. Chem. Int. Ed. Engl. *61*, e202115409. https://doi.org/10.1002/anie.202115409.
59. Nie, Z., Zhang, L., Ding, X., Cong, M., Xu, F., Ma, L., Guo, M., Li, M., and Zhang, L. (2022). Catalytic Kinetics Regulation for Enhanced Electrochemical Nitrogen Oxidation by Ru-Nanoclusters-Coupled Mn3O4 Catalysts Decorated with Atomically Dispersed Ru Atoms. Adv. Mater. *34*, e2108180. https://doi.org/10.1002/adma.202108180.
60. Bose, S., Mofidfar, M., and Zare, R.N. (2024). Direct Conversion of N2 and Air to Nitric Acid in Gas–Water Microbubbles. J. Am. Chem. Soc. *146*, 27964–27971. https://doi.org/10.1021/jacs.4c11899.
61. Dong, K., Yao, Y., Li, H., Li, H., Sun, S., He, X., Wang, Y., Luo, Y., Zheng, D., Liu, Q., et al. (2024). H2O2-mediated electrosynthesis of nitrate from air. Nat. Synth. *3*, 763–773. https://doi.org/10.1038/s44160-024-00522-8.
62. Iriawan, H., Andersen, S.Z., Zhang, X., Comer, B.M., Barrio, J., Chen, P., Medford, A.J., Stephens, I.E.L., Chorkendorff, I., and Shao-Horn, Y. (2021). Methods for nitrogen activation by reduction and oxidation. Nat. Rev. Methods Primers *1*, 56. https://doi.org/10.1038/s43586-021-00053-y.
63. Kresse, G., and Furthmüller, J. (1996). Efficiency of ab-initio total energy calculations for metals and semiconductors using a plane-wave basis set. Comput. Mater. Sci. *6*, 15–50. https://doi.org/10.1016/0927-0256(96)00008-0.
64. Perdew, J.P., Burke, K., and Ernzerhof, M. (1996). Generalized Gradient Approximation Made Simple. Phys. Rev. Lett. *77*, 3865–3868. https://doi.org/10.1103/PhysRevLett.77.3865.
65. Grimme, S., Antony, J., Ehrlich, S., and Krieg, H. (2010). A consistent and accurate ab initio parametrization of density functional dispersion correction (DFT-D) for the 94 elements H-Pu. J. Chem. Phys. *132*, 154104. https://doi.org/10.1063/1.3382344.
66. Momma, K., and Izumi, F. (2008). VESTA: a three-dimensional visualization system for electronic and structural analysis. J. Appl. Crystallogr. *41*, 653–658. https://doi.org/10.1107/S0021889808012016.

Joule, Volume *9*

Supplemental information

Geological ammonia: Stimulated NH_3 production from rocks

Yifan Gao, Ming Lei, Bachu Sravan Kumar, Hugh Barrett Smith, Seok Hee Han, Lokesh Sangabattula, Ju Li, and Iwnetim I. Abate

Supplemental Information

Supplementary Materials

Figures S1 to S13

Table S1 and S2

Supplementary Notes 1 to 5

Supplemental references

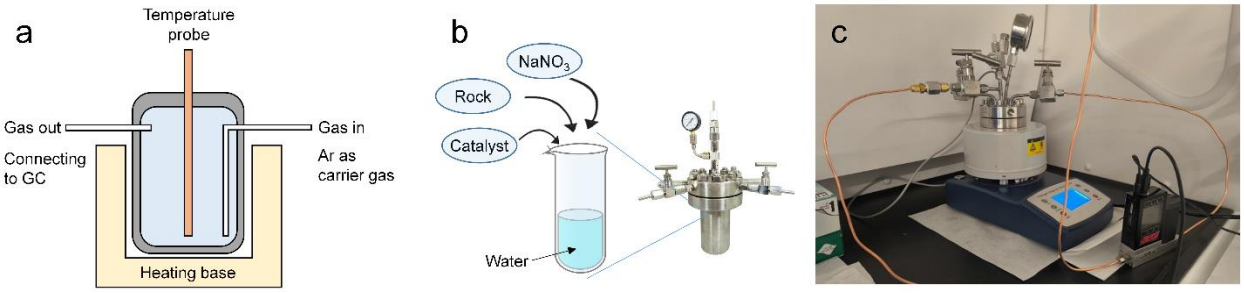

Figure S1. A laboratory-scale rock-water reaction system. (**a** and **b**) Schematic and (**c**) photo of the rock-water reaction system.

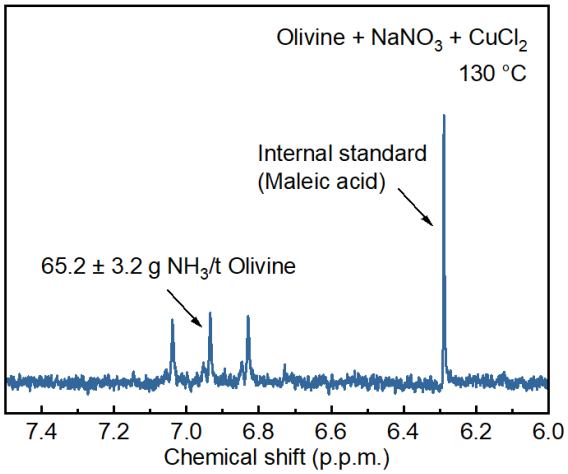

Figure S2. NMR confirmation of NH_3 generation from olivine with Cu^{2+} as a catalyst at 130 °C and 0.25 MPa after 21 h reaction (Higher ammonia yield than Ni^{2+}-catalyzed).

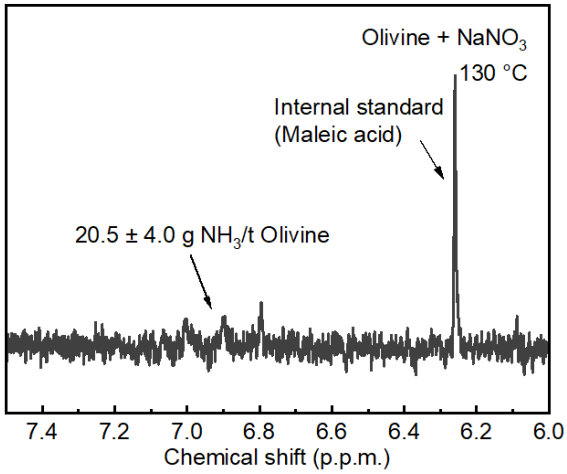

Figure S3. NMR confirmation of NH_3 generation from Olivine without catalyst at 130 °C and 0.25 MPa after 21 h reaction.

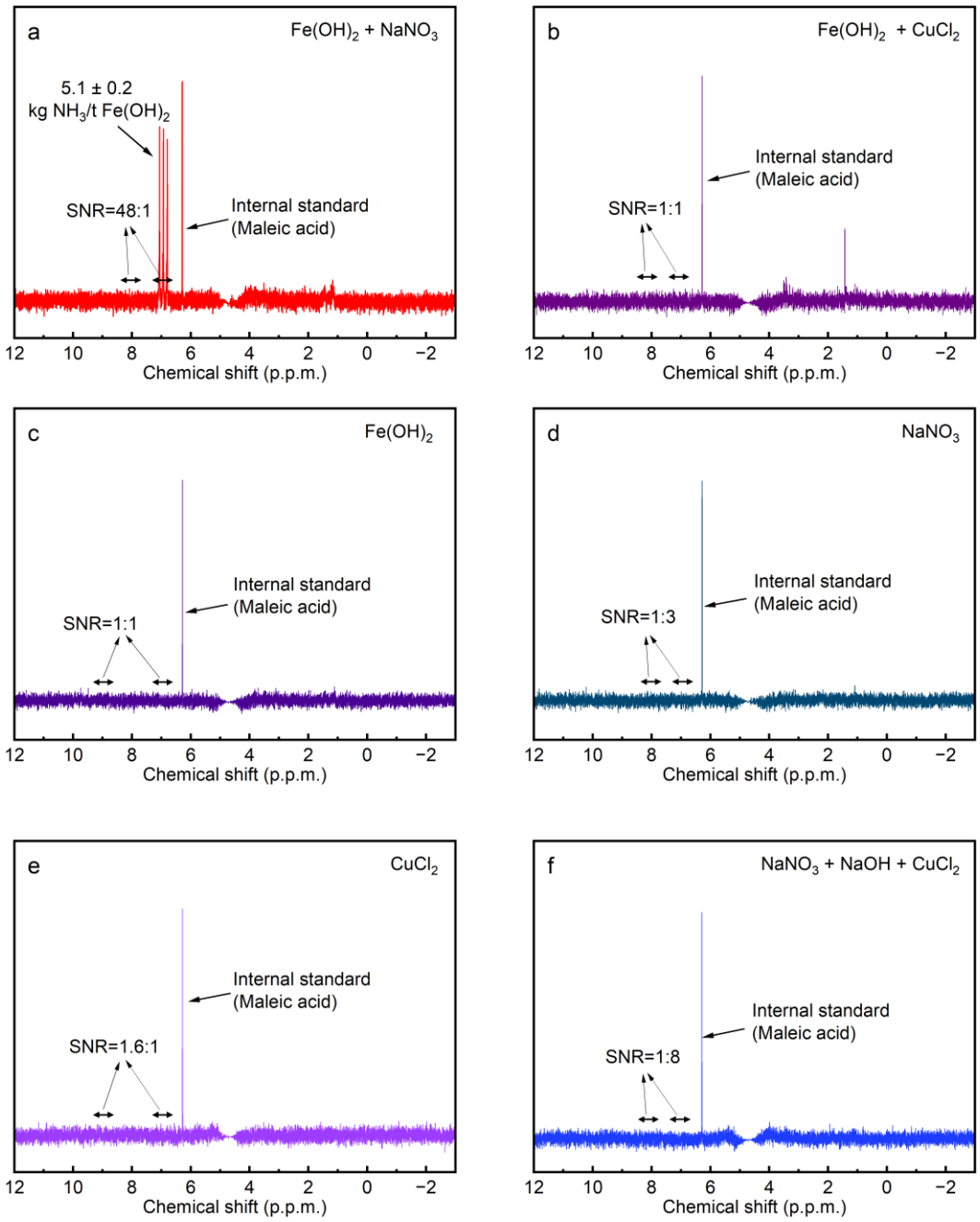

Figure S4. A series of controlled experiments confirmed that NH_3 did come from the reaction of rock with nitrate solution. Ammonia production from the model chemicals reacting under different conditions: (**a**) $Fe(OH)_2$ and $NaNO_3$ were added; (**b**) $Fe(OH)_2$ and $CuCl_2$ were added; (**c**) $Fe(OH)_2$ only; (**d**) $NaNO_3$ only; (**e**) $CuCl_2$ only; and (**f**) $NaNO_3$, NaOH and $CuCl_2$ were added. SNR, i.e. signal-to-noise ratio, demonstrates in detail whether NH_3 is produced or not. All experiments were conducted in 10 minutes under ambient conditions.

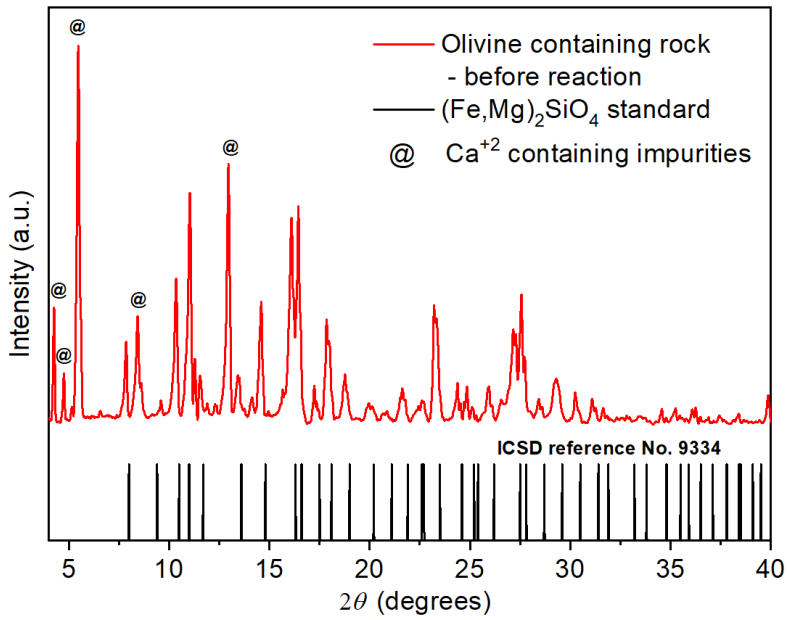

Figure S5. X-ray diffraction pattern for the olivine before the reaction; with the markups showing $(Fe,Mg)_2SiO_4$.

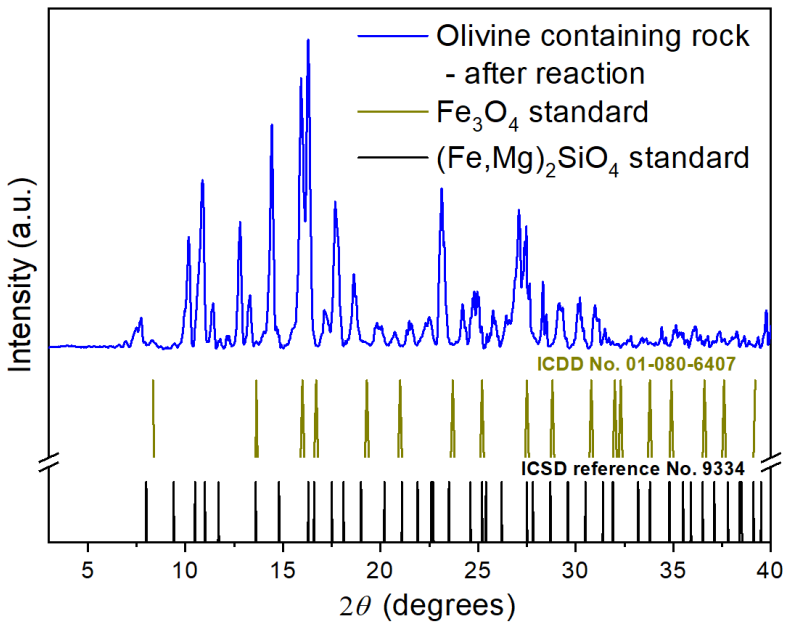

Figure S6. X-ray diffraction pattern for the olivine after the reaction; with the markups showing $(Fe,Mg)_2SiO_4$ and Fe_3O_4.

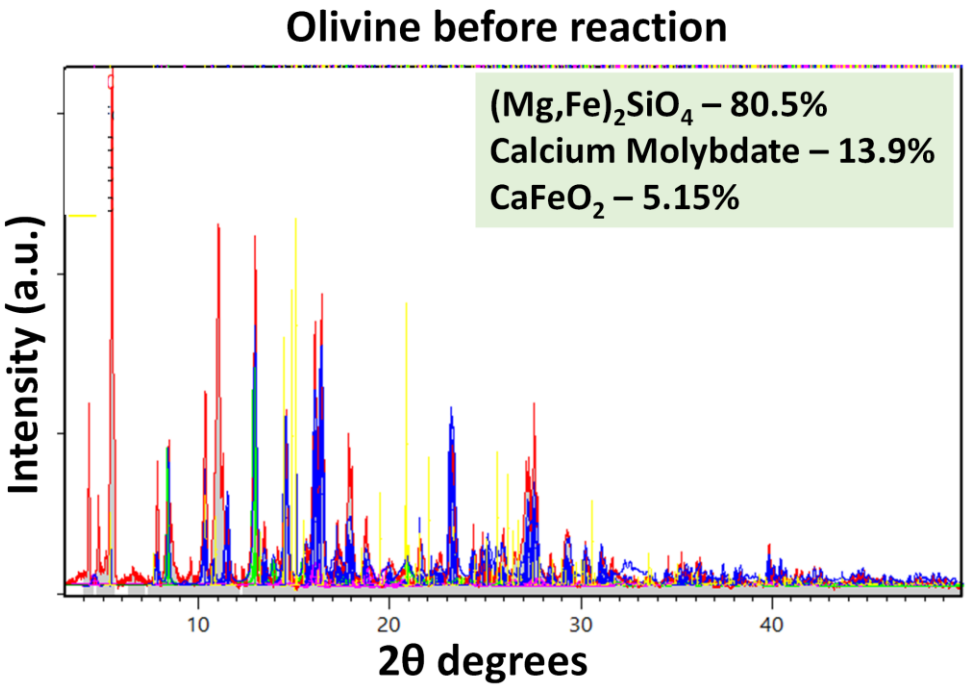

Figure S7. Reitveld refinement of XRD pattern for olivine containing rock before reaction for quantification of different phases.

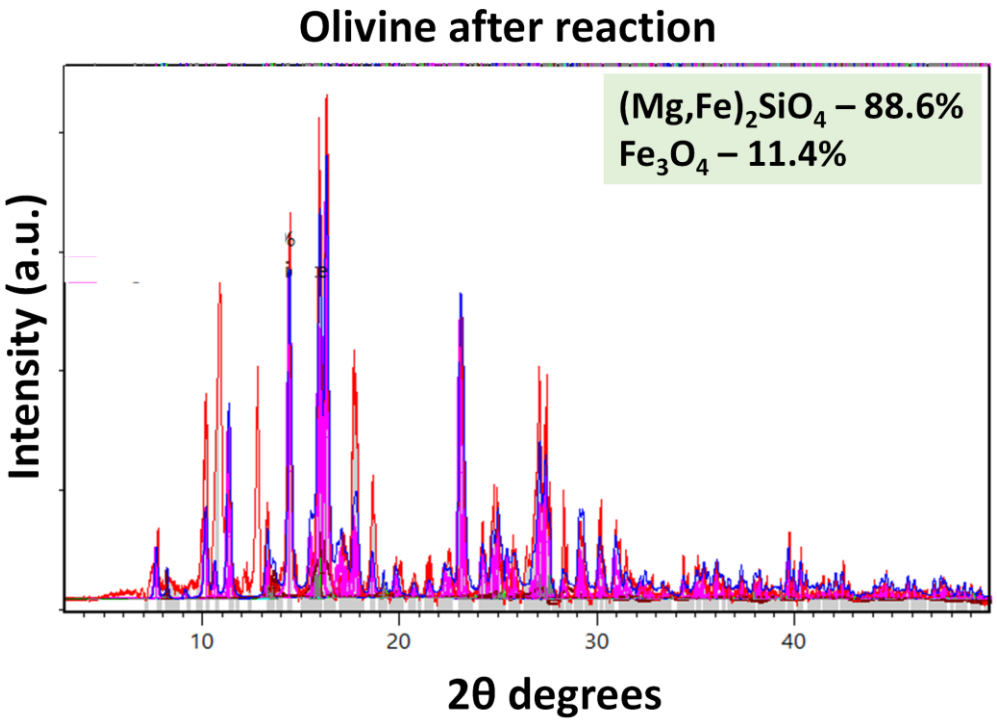

Figure S8. Reitveld refinement of XRD pattern for olivine containing rock after reaction for quantification of different phases.

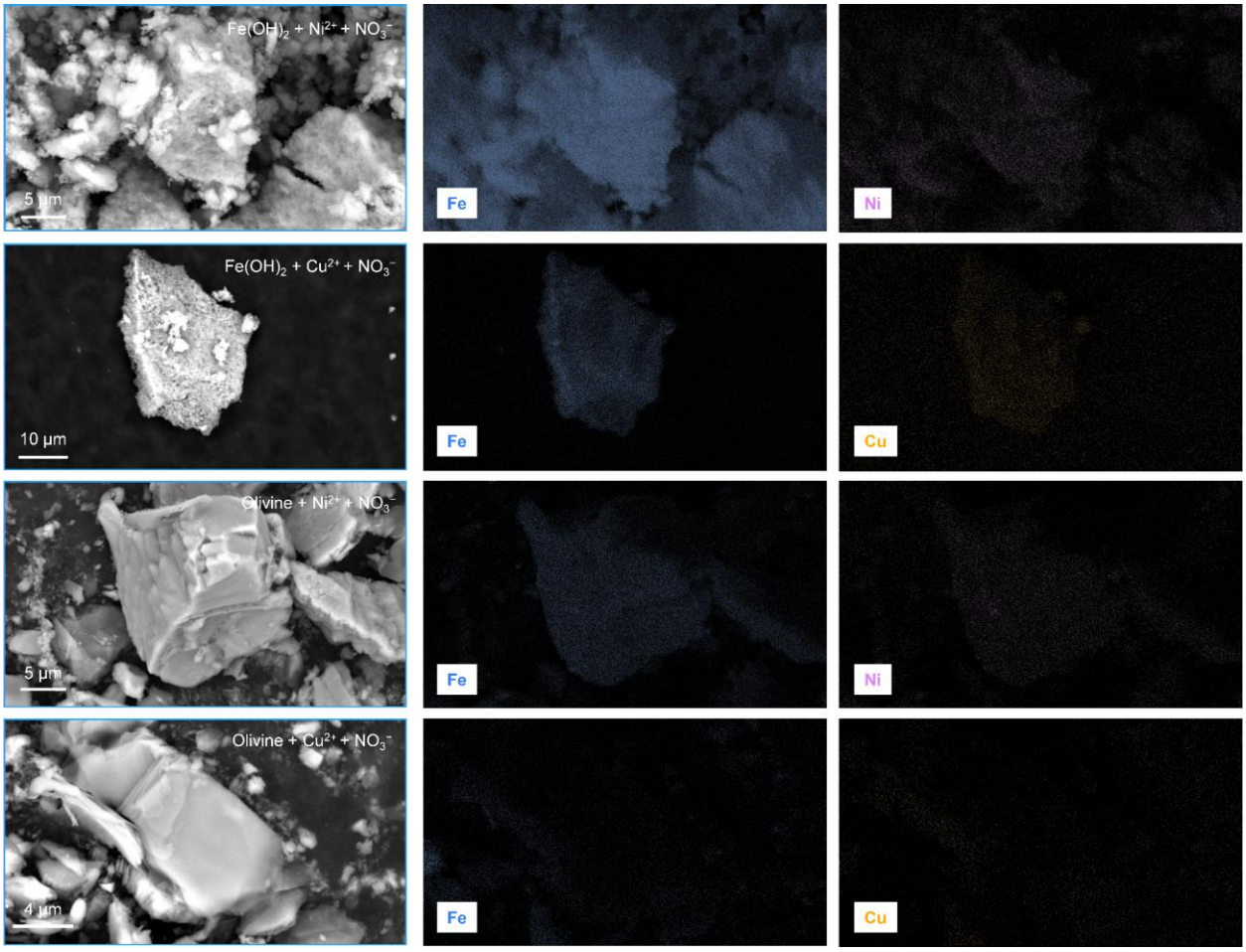

Figure S9. Scanning electron microscope (SEM)-energy dispersive spectrometer (EDS) images showing the co-existence of Fe with Ni or Cu in the reacted rock samples.

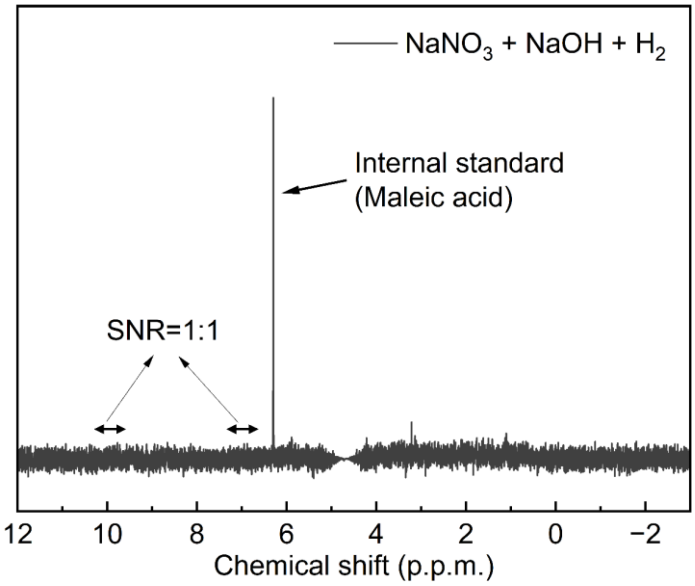

Figure S10. Result of control experiment using $NaNO_3$ and NaOH with H_2 purging for 30 minutes under ambient conditions. NMR pattern results indicated no NH_3 production. SNR, i.e. signal-to-noise ratio, demonstrates in detail whether NH_3 is produced or not.

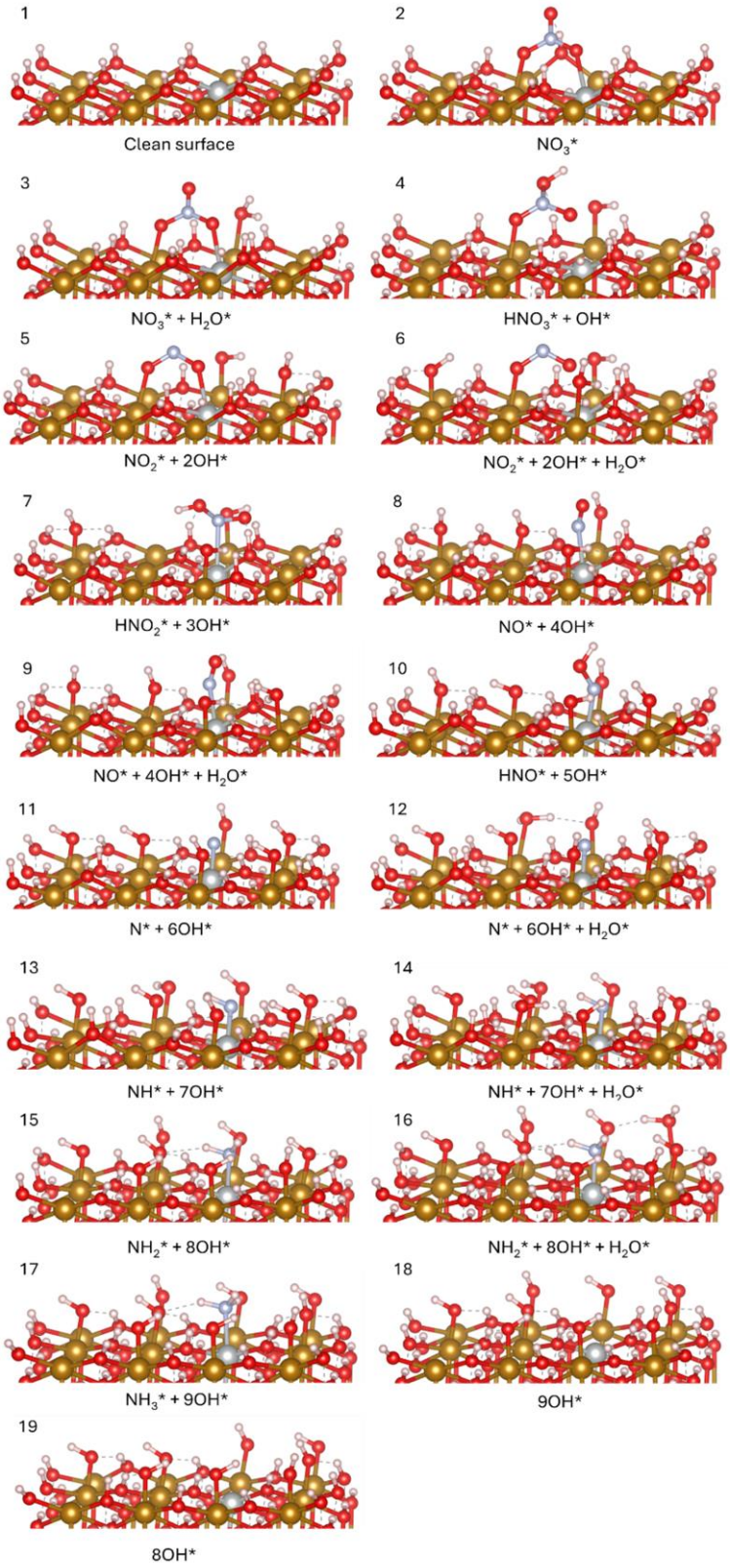

Figure S11. Reaction intermediates along the ammonia generation path (1–19). (Yellow: Fe; Grey: Ni; Light blue: N; Red: O; White: H)

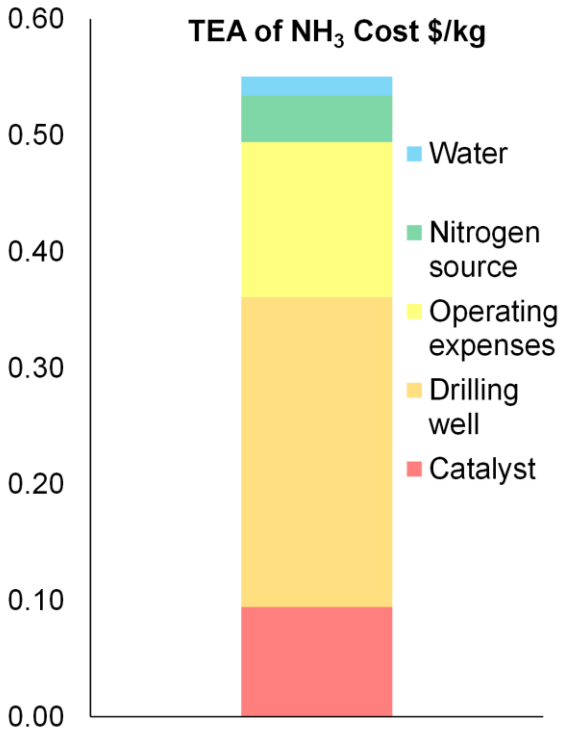

Figure S12. Techno-economic analysis (TEA) calculation of Geo-NH_3.

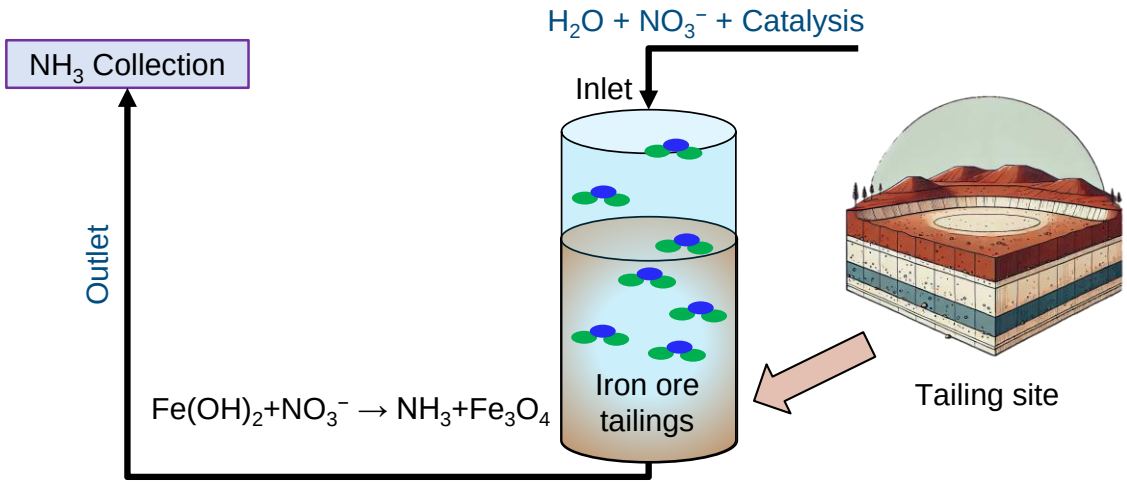

Figure S13. Schematic of the on-ground scale up Geo-NH_3 production from mined Fe^{2+}-containing rocks.

Table S1. Summary of Geo-NH_3 production under different conditions

No.	Reactants	Temperature and pressure	Geo-NH_3 production
1	Olivine + $NaNO_3$ + Cu^{2+}	300 °C, 8.5 MPa	1752.6 ± 96.9 g NH_3/t of olivine
2	Olivine + $NaNO_3$ + Cu^{2+}	130 °C, 0.25 MPa	65.2 ± 3.2 g NH_3/t of olivine
3	Olivine + $NaNO_3$ + Ni^{2+}	130 °C, 0.25 MPa	38.5 ± 3.1 g NH_3/t of olivine
4	Olivine + $NaNO_3$	130 °C, 0.25 MPa	20.5 ± 4.0 g NH_3/t of olivine
5	$Fe(OH)_2$ + $NaNO_3$ + Cu^{2+}	Room T and P	10.4 ± 0.5 kg NH_3/t of $Fe(OH)_2$
6	$Fe(OH)_2$ + $^{15}NaNO_3$ + Cu^{2+}	Room T and P	10.6 ± 0.9 kg $^{15}NH_3$/t of $Fe(OH)_2$
7	$Fe(OH)_2$ + $NaNO_3$ + Ni^{2+}	Room T and P	5.9 ± 0.1 kg NH_3/t of $Fe(OH)_2$
8	$Fe(OH)_2$ + $NaNO_3$	Room T and P	5.1 ± 0.2 kg NH_3/t of $Fe(OH)_2$
9	$Fe(OH)_2$ + $NaNO_3$ + Ni^{2+}	90 °C, 0.1 MPa	7.7 ± 0.4 kg NH_3/t of $Fe(OH)_2$
10	$Fe(OH)_2$ + Cu^{2+}	Room T and P	0
11	$Fe(OH)_2$	Room T and P	0
12	$NaNO_3$	Room T and P	0
13	Cu^{2+}	Room T and P	0
14	NaOH + $^{15}NaNO_3$ + Cu^{2+}	Room T and P	0
15	NaOH + $^{15}NaNO_3$ + Cu^{2+} + H_2	Room T and P	0

Table S2. TEA calculation comparing our method with other NH_3 production pathways

Production Color	Net Energy Input, GJ/t	Direct CO_2 Emissions, tCO_2 eq/t	Price, $/t
Gray (Haber-Bosch)	-8.8	1.6-1.8	400
Blue (Haber-Bosch+ CO_2 sequestration)	-11.2	0.1-0.2	800
Turquoise (Pyrolysis + Haber Bosch)	-28.5	0.2-0.6	800
Green (Electrochemistry)	-15.6	0.12-0.53	2170[1]
Orange (This work)	17.5	<0.1	550

Supplementary Note 1. Detailed discussion of the differences between various ammonia production technologies

Our work demonstrates a novel approach to ammonia production directly from aqueous nitrate and olivine or $Fe(OH)_2$ under ambient or very accessible underground conditions (130 °C–300 °C), without the need for high energy input or electricity or any additional H_2.

Traditionally, ammonia (NH_3) is synthesized through the Haber-Bosch process, which uses N_2 and H_2 and operates under high temperatures (400 °C–500 °C) and high pressures (150 atm–200 atm) with an iron-based catalyst. Another method involves the electroreduction of nitrate in solution, which may offer higher yields with fewer environmental risks. But both pathways require substantial energy consumption, whether through additional H_2 or electricity.

In addition to the innovation of no H_2 or electricity required, and operating under ambient conditions or very accessible underground conditions (130 °C–300 °C), our work also introduces a novel process for the geological reduction of nitrate. It is worth noting that almost all current research focuses on the electrocatalytic reduction of nitrate, whereas our study is among the few that use the reducing ability of rocks for this purpose.

In the electroreduction of nitrate to produce NH_3, (or generally speaking, in the theoretical studies of electrocatalysis), the reaction mechanisms typically do not need to consider the transfer of electrons between the electrode and the reactants, and the sources of reactants (H^+ and OH^-). These species usually diffuse from the solution phase to the electrode surface or desorb from the electrode surface after generation and then diffuse into the bulk solution. For example, the proposed mechanisms include:

$NO_3^- \rightarrow *NO_3 \rightarrow *NO_2 \rightarrow *NO \rightarrow *N \rightarrow *NH \rightarrow *NH_2 \rightarrow *NH_3 \rightarrow NH_3(g)$[2,3]

$NO_3^- \rightarrow *NO_3 \rightarrow *NO_2 \rightarrow *NO \rightarrow *NOH \rightarrow *NHOH \rightarrow *NH_2OH \rightarrow *NH_2 \rightarrow *NH_3 \rightarrow NH_3(g)$[4]

In order to efficiently perform electrochemical reactions, a highly concentrated electrolyte solution is usually necessary to guarantee rapid electron transfer, i.e. a high salt concentration in the water is required. In addition, since all electrochemical reactions are electrode interface reactions, while the electrode area is much smaller than the area of the bulk phase in solution. Therefore a high concentration of reactants (i.e., nitrates) is also required to sustain a fast reaction. Although H_2 is not required for the production of NH_3 from electrocatalytic reduction of nitrate, the high conductivity and high nitrate concentration requirements of the feedstock aqueous solution as well as the consumption of electrical energy are challenges[5]. Especially when considering the use of nitrate-containing wastewater as a feedstock, this challenge is difficult to

overcome: both the salt and nitrate concentrations of the wastewater are typically too low to meet the requirements. The use of processes such as electrodialysis (ED) to firstly concentrate the low NO_3^- sources into target concentrations prior to electrocatalytic reduction of nitrate solutions has often been proposed[1,6].

The Geo-NH_3 production presented in our study is non-electrochemical chemical redox reaction. This reaction is completely independent of the conductivity of the solution and can work well for low nitrate concentrations (will be shown later). Non-electrochemical also means that the process is not dependent on electrical energy at all, making it more suitable for decentralized NH_3 production and significantly reducing both capital and operation and maintenance costs.

Besides, through rigorous experimental and computational investigation (see **Main Text** and **Fig. 4** for more discussion), we proposed a reaction mechanism:

$$12Fe(OH)_2 + 6H_2O + NO_3^- \rightarrow NH_3 + 4Fe_3O_4 + 16H_2O + OH^-$$

Thermodynamic energy analysis from our DFT calculation suggest H for nitrate reduction comes from the dissociation of H_2O molecules. Previous experimental research on hydrogen production using olivine or $Fe(OH)_2$ has also demonstrated that the hydrogen comes from H_2O molecules rather than from olivine or $Fe(OH)_2$ itself using isotopic measurements[7]. Moreover, even though the dissociation of H_2O molecules is an endothermic reaction with a large ΔG (greater than 2 eV)[7,8], our calculations found that the reaction between the dissociated H from H_2O and the reaction intermediates (such as $*NO_3$, $*NO_2$, *NO, *N) facilitates the dissociation of H_2O (lowering the ΔG to less than 2 eV) (see **Main Text** and **Fig. 4** for more discussion).

Supplementary Note 2. Details on Generation of H_2 and NH_3 from rock

As shown in **Fig. 2c**, very low H_2 generation was observed in the presence of nitrate even with the catalyst (magenta color). When nitrate is present, the NH_3-producing reaction significantly dominates the H_2-producing reaction. After 300 minutes trace production of H_2 (about 2.5 μmol) was observed. The possible reason one is that after 300 minutes, the generated Fe_3O_4 may have prevented further reduction of NO_3^- to NH_3, but H_2O can start slightly enter the interface to react with the internal $Fe(OH)_2$ to produce H_2. Second, previous studies on Geo-H_2 have reported that the rock-water reaction leads to chemo-mechanics, where the rocks expand in volume, causing cracking and creating new surfaces for the reaction[9]. In our case, it may be possible that after 6 hours of Geo-NH_3, similar chemo-mechanics occur, exposing new surfaces for H_2O to be

reduced to H_2. However, by this time, we may have consumed most of the NO_3^-, which could otherwise compete to produce NH_3.

Supplementary Note 3. Details on the systematic controlled experiments rule out the possibility of false-positive NH_3 production

The result in **Fig. S4b** was from an experiment with no nitrate added and all other conditions being the same. The absence of ammonia production is an evidence that there are no impurities or side reactions in the reactants and experimental system other than nitrate. And **Fig. S4d** shows the result of a pure nitrate solution under the same conditions, proving that the nitrate itself does not produce ammonia, and that there are no impurities or side reactions. Combining **Fig. 2e** (positive results), **Fig. S4b** (negative results), **Fig. S4d** (negative results), and **Fig. 2f** (positive isotopic $^{15}NH_3$ production) is a classic systematic investigation of controlled experiments in NH_3 production studies[10]. Furthermore, we have also investigated the absence of NH_3 impurities in both pure $Fe(OH)_2$ (**Fig. S4c**) and pure Cu^{2+} (**Fig. S4e**), as well as the absence of NH_3 production in the absence of Fe^{2+} in the system (**Fig. S4f**).

Supplementary Note 4. Details on density functional theory (DFT) calculations

Due to the significant differences in the crystal phases of $Fe(OH)_2$ and Fe_3O_4, simulating the phase transition during the reaction pathway is challenging. Instead, we consider the following simplified reaction (Eq. S1):

$$12Fe(OH)_2 + 6H_2O + NO_3^- \rightarrow NH_3 + Fe_{12}(OH)_{24}(OH)_8 + OH^- \quad \text{(Eq. S1)}$$

In both Fe_3O_4 and $Fe_{12}(OH)_{24}(OH)_8$, the Fe ions are in the +8/3 oxidation state. The decomposition of $Fe_{12}(OH)_{24}(OH)_8$ produces Fe_3O_4:

$$Fe_{12}(OH)_{24}(OH)_8 \rightarrow 4Fe_3O_4 + 16H_2O \quad \text{(Eq. S2)}$$

In other words, in our calculations, we neglect the surface decomposition of $Fe_{12}(OH)_{24}(OH)_8$ (water generation) and the phase reconstruction process.

The elementary steps of the overall reaction are as follows (reaction intermediates showed in **Fig. S11**):

$$NO_3^- + * \rightarrow NO_3* \quad \text{(Eq. S3)}$$

$$NO_3* + H_2O + * \rightarrow NO_3* + H_2O* \quad \text{(Eq. S4)}$$

$$NO_3* + H_2O* \rightarrow HNO_3* + OH* \quad \text{(Eq. S5)}$$

$$HNO_3* + OH* \rightarrow NO_2* + 2OH* \quad \text{(Eq. S6)}$$

$NO_2^* + 2OH^* + H_2O^* \rightarrow HNO_2^* + 3OH^*$ (Eq. S7)

$HNO_2^* + 3OH^* \rightarrow NO^* + 4OH^*$ (Eq. S8)

$NO^* + 4OH^* + H_2O^* \rightarrow HNO^* + 5OH^*$ (Eq. S9)

$HNO^* + 5OH^* \rightarrow N^* + 6OH^*$ (Eq. S10)

$N^* + 6OH^* + H_2O^* \rightarrow NH^* + 7OH^*$ (Eq. S11)

$NH^* + 7OH^* + H_2O^* \rightarrow NH_2^* + 8OH^*$ (Eq. S12)

$NH_2^* + 8OH^* + H_2O^* \rightarrow NH_3^* + 9OH^*$ (Eq. S13)

$NH_3^* + 9OH^* \rightarrow NH_3(g) + 9OH^*$ (Eq. S14)

$NH_3(g) + 9OH^* \rightarrow NH_3(g) + 8OH^* + OH^-$ (Eq. S15)

Some steps, such as those described in Eq. S5 and S9, exhibit large free energy changes. These steps involve water dissociation, which results in a substantial ΔG. Song et al.[7] calculated the water dissociation reaction on the (100) surface of $Fe(OH)_2$ and Ni-doped $Fe(OH)_2$, finding ΔG values of 2.17 and 1.51 eV, respectively. In our ammonia generation reaction, when combined with nitrate reduction, the ΔG for water dissociation decreases to 1.66 eV (Eq. S5) and 2.01 eV (Eq. S9) on the $Fe(OH)_2$ surface, and 1.51 eV (Eq. S5) and 1.96 eV (Eq. S9) on the Ni-doped $Fe(OH)_2$ surface (with these steps occurring away from the Ni atom).

Besides the water dissociation steps, the desorption of ammonia and hydroxyl ion also shows large free energy changes. The desorption energies of ammonia on $Fe(OH)_2$ and Ni-doped $Fe(OH)_2$ surfaces are 1.27 and 1.38 eV, respectively. The desorption energies of hydroxyl ion on $Fe(OH)_2$ and Ni-doped $Fe(OH)_2$ surface are 2.66 and 2.47 eV, respectively. Considering Eq. S2, we suggest that the desorption of hydroxyl ions is likely easier. It is worth noting that our calculations assume an ideal condition where all the H comes from the dissociation of H_2O. However, it is also possible that H comes from H^+ in acid solution or OH^- in an alkaline solution. In such a case, the ΔG of those elementary reaction steps would decrease even further. Realistically, calculations cannot fully account for this scenario due to the numerous possible intermediate processes.

Supplementary Note 5. Details on the techno-economic outlook

The techno-economic analysis (TEA) leverages oil & gas waterflood techniques and enhanced geothermal parallels to estimate an injector/producer pair for stimulating and collecting subsurface ammonia production. The TEA is based on accessing a large volume of subsurface rock to react with nitrate by constructing an average wellbore using West Texas publicly available data and estimated rock properties of the formation, including an expected stimulated rock volume from

a hydraulic fracture treatment. This ultimately allows for a calculation of the accessible iron available that can be reacted to form ammonia and cumulative ammonia production per well pair. Well capital expenditure is based on the typical well geometries within the Permian Basin. Key variables within the techno-economic analysis include the ferrous iron concentration, the size of the iron formation, and stimulated rock volume. Secondary factors include required catalyst concentration, catalyst price, drilling capital, and nitrate price.

First, for the use of nitrate as a nitrogen source, based on our NH_3 yield in the lab and given further optimization of conditions, the cost of wells (drilling and cracking of rock, etc.) is about \$0.267/kg NH_3[11]. The operating expenses is about \$0.133/kg NH_3. Based on the catalyst additions in our experiments and the catalyst price[12], the cost of catalysts is about \$0.094/kg NH_3. In addition, the cost of nitrate feedstock is \$0.04 /kg NH_3, based on utilizing wastewater containing nitrates and considering costs such as transportation, etc. The chemical reaction (Eq. 8 in the Main text) to produce Geo-NH_3 does not consume water. Considering the losses in the water recycling process, the cost of water[13] is about \$0.0162 /kg NH_3. Taking these values together, the cost of Geo-NH_3 can be derived as \$0.55 per kg of NH_3. Moreover, if the Geo-NH_3 reaction is performed on ultramafic rock formation naturally containing Ni or Cu catalysts (already identified in Costa Rica, Oregon, and California[14]), then this cost can be reduced to \$0.46 per kg NH_3.

When the nitrogen source is changed from nitrate to N_2 gas, the calculation process is similar. Only the chemical reaction equation based on it has changed, so that around 14 kg of Geo-NH_3 can be produced per tonne of rock. Besides, 0.93 kg of N_2 is required for the production of each kg of Geo-NH_3. All other values and calculations are similar to where the nitrate as a nitrogen source, resulting in a Geo-NH_3 cost of \$0.3–\$0.5/kg NH_3.

References

1. Chen, F.-Y., Elgazzar, A., Pecaut, S., Qiu, C., Feng, Y., Ashokkumar, S., Yu, Z., Sellers, C., Hao, S., Zhu, P., et al. (2024). Electrochemical nitrate reduction to ammonia with cation shuttling in a solid electrolyte reactor. Nat. Catal. *7*, 1032–1043. https://doi.org/10.1038/s41929-024-01200-w.

2. Wang, Y., Xu, A., Wang, Z., Huang, L., Li, J., Li, F., Wicks, J., Luo, M., Nam, D.-H., Tan, C.-S., et al. (2020). Enhanced Nitrate-to-Ammonia Activity on Copper–Nickel Alloys via Tuning of Intermediate Adsorption. J. Am. Chem. Soc. *142*, 5702–5708. https://doi.org/10.1021/jacs.9b13347.

3. Liu, J.-X., Richards, D., Singh, N., and Goldsmith, B.R. (2019). Activity and Selectivity Trends in Electrocatalytic Nitrate Reduction on Transition Metals. ACS Catal. *9*, 7052–7064. https://doi.org/10.1021/acscatal.9b02179.

4. Wang, Y., Zhou, W., Jia, R., Yu, Y., and Zhang, B. (2020). Unveiling the Activity Origin of a Copper-based Electrocatalyst for Selective Nitrate Reduction to Ammonia. Angew. Chem. Int. Ed. *59*, 5350–5354. https://doi.org/10.1002/anie.201915992.

5. van Langevelde, P.H., Katsounaros, I., and Koper, M.T.M. (2021). Electrocatalytic Nitrate Reduction for Sustainable Ammonia Production. Joule *5*, 290–294. https://doi.org/10.1016/j.joule.2020.12.025.

6. Chen, Y., Ammari-Azar, P., Liu, H., Lee, J., Xi, Y., Castellano, M.J., Gu, S., and Li, W. (2023). Sustainable waste-nitrogen upcycling enabled by low-concentration nitrate electrodialysis and high-performance ammonia electrosynthesis. EES Catal. *1*, 504–515. https://doi.org/10.1039/D3EY00058C.

7. Song, H., Ou, X., Han, B., Deng, H., Zhang, W., Tian, C., Cai, C., Lu, A., Lin, Z., and Chai, L. (2021). An Overlooked Natural Hydrogen Evolution Pathway: Ni2+ Boosting H2O Reduction by Fe(OH)2 Oxidation during Low-Temperature Serpentinization. Angew. Chem. Int. Ed. *60*, 24054–24058. https://doi.org/10.1002/anie.202110653.

8. Li, Y.-F., Liu, Z.-P., Liu, L., and Gao, W. (2010). Mechanism and Activity of Photocatalytic Oxygen Evolution on Titania Anatase in Aqueous Surroundings. J. Am. Chem. Soc. *132*, 13008–13015. https://doi.org/10.1021/ja105340b.

9. Plümper, O., Røyne, A., Magrasó, A., and Jamtveit, B. (2012). The interface-scale mechanism of reaction-induced fracturing during serpentinization. Geology *40*, 1103–1106. https://doi.org/10.1130/G33390.1.

10. Iriawan, H., Andersen, S.Z., Zhang, X., Comer, B.M., Barrio, J., Chen, P., Medford, A.J., Stephens, I.E.L., Chorkendorff, I., and Shao-Horn, Y. (2021). Methods for nitrogen activation by reduction and oxidation. Nat. Rev. Methods Primer *1*, 56. https://doi.org/10.1038/s43586-021-00053-y.

11. Estay, H., Díaz-Quezada, S., Arancibia, E., and Vargas, T. (2023). Economic Assessment of an In Situ Leaching Operation with Ore Preconditioning Using Sublevel Stoping Techniques. Min. Metall. Explor. *40*, 493–504. https://doi.org/10.1007/s42461-023-00736-y.

12. Wikipedia. Prices of chemical elements. https://en.wikipedia.org/w/index.php?title=Prices_of_chemical_elements&oldid=1243958447.

13. Unger, S.R., Kilgannon, E.M., Elliott, D.B., Cort, K.A., and Stoughton, K.L.M. (2023). Water and Wastewater Annual Price Escalation Rates for Selected Cities Across the United States: 2023 Edition (Pacific Northwest National Laboratory (PNNL), Richland, WA (United States)) https://doi.org/10.2172/1975260.

14. Schwarzenbach, E.M., Caddick, M.J., Beard, J.S., and Bodnar, R.J. (2015). Serpentinization, element transfer, and the progressive development of zoning in veins: evidence from a partially serpentinized harzburgite. Contrib. Mineral. Petrol. *171*, 5. https://doi.org/10.1007/s00410-015-1219-3.